Univerzita Karlova

Přírodovědecká fakulta

Studijní program: Chemie

Studijní obor: Medicinální chemie

Eva Hlavatovičová

Kompartmentalizované nanočástice tvořené ABC trojblokovými terpolymery jako potenciální nosiče léčiv

Multicompartment nanoparticles based on ABC triblock terpolymers as potential drug delivery vehicles

Bakalářská práce

Školitel: Ing. Mariusz Uchman Ph.D.

Konzultant: doc. RNDr. Pavel Matějíček, Ph.D.

Praha, 2018

Prohlášení:

Prohlašuji, že jsem závěrečnou práci zpracovala samostatně a že jsem uvedla všechny použité informační zdroje a literaturu. Tato práce ani její podstatná část nebyla předložena k získání jiného nebo stejného akademického titulu.

V Praze, dne 17.05.2018

I would like to thank to my supervisor Ing. Mariusz Uchman Ph.D. and my advisor doc. RNDr. Pavel Matějíček, Ph.D., for the great opportunity to be part of their research group and for their patient guidance, encouragement and motivation for science since the beginning of my studies. I would also thank to doc. RNDr. Miroslav Štěpánek Ph.D. for offering me help in fluorescence and light scattering, to all my colleagues for the continuous help, especially Roberto Fernandez Alvarez and Vladimír Ďorďovič. Special thanks go to my family for the support and encouragements throughout my study.

Abstrakt

Bakalářská práce se zabývá studiem nanočástic připravených z nově syntetizovaného amfifilního trojblokového terpolymeru, poly(akrylová kyselina)-b-poly(4-hydroxystyren)-*b*-poly(karboranyl-styren). Reprodukovatelnou metodou byly připraveny různé typy kompartmentalizovaných nanočástic s obsahem sloučenin bóru (kulovité micely, cylindrické částice) v závislosti na složení selektivního rozpouštědla a s tím souvisejících solvofobně-solvofilních sil. Velikost, tvar a vnitřní struktura nanočástic byly analyzovány pomocí technik rozptylu světla, fluorometrie a mikroskopie cryo-TEM. Rozpustnost dvou modelových léčiv (fluoroforů 2-methylnaftalen a 7-metoxykumarin-o-karboran) v jednotlivých kompartmentech byla studována pomocí fluorometrie s cílem možného využití nanočástic s obsahem karboranových klastrů jako duálních nosičů léčiv.

Abstract

This thesis deals with the self-assembly behavior of newly synthetized well-defined amphiphilic poly(acrylic acid)-*b*-poly(4-hydroxystyrene)-*b*-poly(styrene-carborane) triblock terpolymer in aqueous solution. A reproducible method was developed for the preparation of diverse multicompartment boron-containing nanostructures (spherical micelles, wormlike micelles) depending on the initial solvent composition and solvophobic-solvophilic interactions. Self-assembled nanostructures were characterized by various techniques (static and dynamic light scattering, cryogenic transmission-electron microscopy and fluorescence spectroscopy). The solubilization of two model drugs (2-methylnaphtalene and 7-methoxycoumarine-carborane fluorophores) in polymer nanoparticles was studied by fluorescence spectroscopy to investigate its potential in drugs solubilization and delivery.

Abbreviations

AIBN – azobisisobutyronitrile

CTA – chain transfer agent

BNCT – boron-neutron-capture therapy

CBMC – 7-methoxycoumarin-carborane-conjugate based probe

CMC – critical micelle concentration

CONTIN – constrained inverse Laplace transform routine

Cryo-EM – cryogenic electron microscopy

Cryo-SEM – cryogenic scanning electron microscopy

Cryo-TEM – cryogenic transmission electron microscopy

DLS – dynamic light scattering

EPR – enhanced permeability and retention effect

FRET – fluorescence resonance emission transfer

I – initiator

N – 2-methyl naphthalene

NMR – nuclear magnetic resonance (spectroscopy)

PAA – poly(acrylic acid)

PAOS – poly(4-acetoxystyrene)

PHS – poly(4-hydroxystyrene)

PSC – poly(styrene-carborane) or poly(carboranyl styrene)

PS – polystyrene

P*t*BA – poly(tert-butyl acrylate)

RAFT – reversible addition-fragmentation chain-transfer polymerization

SC – “styrene-carborane” monomer

SEC – size exclusion chromatography

SLS – static light scattering

Content

1. Introduction

Extensive studies of amphiphilic block copolymers self-assembly over the two past decades led to the refinement of polymer characteristics, technical implementation of self-assembly and the improvement of visualization techniques. The self-organization processes of triblock terpolymer yielding multicompartment micelles tend to mimic biological structures in living organisms with the ability of targeted multiple substance transport.

The self-assembly of ABC triblock terpolymers is highly influenced by the solubility, compatibility and position of individual blocks in polymer chains, which refines organized nanostructures between multiple types of multicompartmental compounds, among them: core-shell-corona micelles, strawberry-like micelles, core and shell compartmentalized micelles. A detailed characterization of newly created morphologies using different techniques, e.g. light scattering, fluorescence spectroscopy or cryogenic transmission electron microscopy helps us define micellar parameters that are necessary for their applications. Individual micellar domains offer the possibility of simultaneous and selective encapsulation of two different active compounds which may find potential use in pharmacology as a drug delivery carrier.

This thesis deals with the self-assembly behavior of newly synthetized ABC triblock terpolymer, poly(acrylic acid)-*b*-poly(4-hydroxystyrene)-*b*-poly(styrene-carborane), *(*PAA-*b*-PHS-*b*-PSC*)*, in aqueous solutions. The formation and structure of nanoassemblies were studied by static and dynamic light scattering, cryogenic transmission-electron microscopy and fluorometry.

2. Review of the literature

2.1. Triblock terpolymers architecture

Controlled polymerization like reversible addition-fragmentation chain-transfer polymerization (RAFT) ensures the control over exact spatial arrangement of polymer and permits to influence the block order in polymer chains. Triblock terpolymers are composed of three various polymer blocks which can be organized into linear, μ-arm, grafted, ring and others block copolymers structures, represented in Figure 1.[1] Block order within individual spatial polymer arrangement can crucially influence its overall properties. Polymer forming blocks, solvophilic A block and two solvophobic blocks B and C, can be organized into ABC, BAC and ACB architecture,[2] Figure 1.

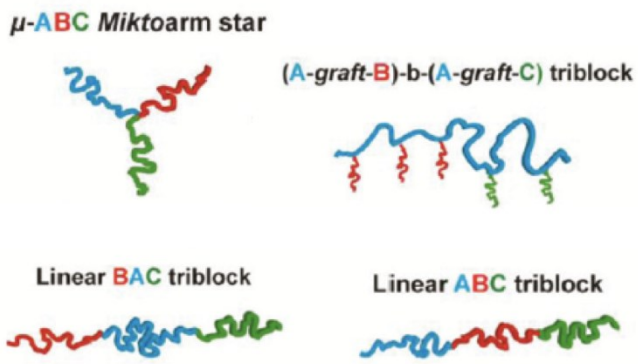

Figure 1 Examples of triblock terpolymer architectures consisting of A, B and C blocks.

2.2. Self-assembly of ABC triblock terpolymers in aqueous solution

The nanostructures obtained from ABC triblock terpolymers depend on various factors: the nature of individual blocks and their compatibility with each other, solvent composition, and temperature. The selection of solvent is a key feature in obtaining novel self-assembly structures, the use of a selective solvent readily provokes the microphase separation. Selective solvent refers to a solvent that is a good solvent for one block and a poor solvent or non-solvent for another one. In general, the AB diblock copolymer in selective solvent for A block can produce three basics morphologies: spherical micelles, worm-like micelles and vesicles (lamellar structures) depending on

relative length of the blocks.[3] In the case of the ABC triblock terpolymer, the complexity of possible nanostructures increases. The typical examples of morphologies produced by triblock terpolymers are as follows: core-shell-corona micelles, core-corona micelles, multicompartment micelles, nanotubes, helices and others. Multicompartment micelles that consist of non-polar separated regions could mimic biological structures such as serum albumins making it possible to transport incompatible hydrophobic substances. The self-association of block copolymers with chemically incompatible blocks occurs in selective solvents. The selection of solvent affects the micelle formation along with the polymer concentration. If water is used as the selective solvent, the hydrophobic effect is the driving force of the self-assembly.[4] Along with the hydrophobic effect, macromolecule association can be driven also by attractive interaction (related to enthalpy of micellization) between segments which is balanced by the repulsive force and the tendency to minimize the micelle surface that prevents unlimited growth of particles. The polymer concentration effect on polymer self-assembly is very similar to the concept of micelle formation of surfactants. A major difference between surfactant molecules and copolymer aggregates is in the size of their building blocks. Copolymers with the molecular weight of a few hundreds of grams per mole are generally two orders of magnitude larger than surfactant molecules. Polymers associate into micellar structures only when their concentration is above the critical micelle concentration (CMC). In general, the CMC for surfactants is higher than for polymers. The association process is driven in the way that the solvophobic (hydrophobic) block is tending to avoid the contact with the solvent in which the polymer is diluted. Those parts of blocks associate to form the micellar core. At CMC, an important quantity of solvent is present inside of micelles that are much larger than micelles formed at higher polymer concentration. Those associates at CMC are called loose aggregates. At higher concentrations, micelles will reach their lowest energy state favored by equilibrium and the solvent molecules inside the micelles will be released from hydrophobic core. That causes the rearrangement of the micellar core leading to the size restriction of micelles. At very low concentrations, polymer chains exist only as single chains.[3,4,5]

In the case of preparation of micelles in water from block copolymer with long hydrophobic block, an important step is to choose the adequate procedure among many possible techniques with respect to the polymer blocks properties. A three-step method for micelle formation is presented as follows. (1) The polymer is dissolved in selective

solvent mixture.[6] Organic solvents and water solution mixtures have been frequently applied as initial solvents for block copolymers that consist of long solvophobic (hydrophobic) block, for example polystyrene (PS). The solvent mixtures ensure the complete dissolution of polymers. (2) As the common solvent is eliminated from the solvent mixture for example by distillation, dissolved polymer chains slowly self-assemble into organized structures. Those assemblies are formed by non-covalent interactions in way to reach the lowest energy and equilibrium state. The micelle size is then influenced by solvent mixture composition. The self-assembly process can be accelerated by reaching the limit where the system becomes kinetically frozen. At this point, the equilibrium between free chains and micelles is blocked. It can be achieved by the drastic change of solvent composition by a prevalent amount of non-solvent for one block or eventually by decreasing the temperature bellow the glass transition temperature of the core forming block. (3) To insure the complete removal of common solvent it is efficient to dialyze the micellar solution against the great amount of water or aqueous buffers.[4,5,6]

2.3. Micellar morphologies from linear triblock terpolymers

Factors affecting morphology of created nanostructures are as already mentioned selectivity of the solvent and polymer concentration. Another very important self-assembly architecture influencing element is the block order in the polymer chain and the compatibility of individual polymer blocks with each other. The ABC and BAC block organization in polymers which undergo self-assembly yield the organization of three blocks into three different micellar domains. Such structures are called multicompartment micelles, which include “sphere in sphere” micelles or strawberry-like micelles. When only two micellar domains from three polymer blocks are formed, as in case of ACB polymer organization, it concerns the core-corona structures. Upon the compatibility of soluble A and B blocks, the corona, obtained morphologies are divided into mixed-corona micelles, segregated-corona micelles and Janus particles.

2.3.1. *Compartmentalized micelles*

The organization of three polymer blocks into three different domains in one nanostructure is considered as a multicompartment morphology of self-assembled structures. The term "multicompartment" stands for the microphase separation of two or more blocks driven by the block incompatibility. The domain formation of highly incompatible blocks can occur within the micellar core or shell, leading to core compartmentalized micelles and shell compartmentalized micelles, respectively.[1,7,8,9,11] The examples of core compartmentalized micelles are shown in Figure 2.

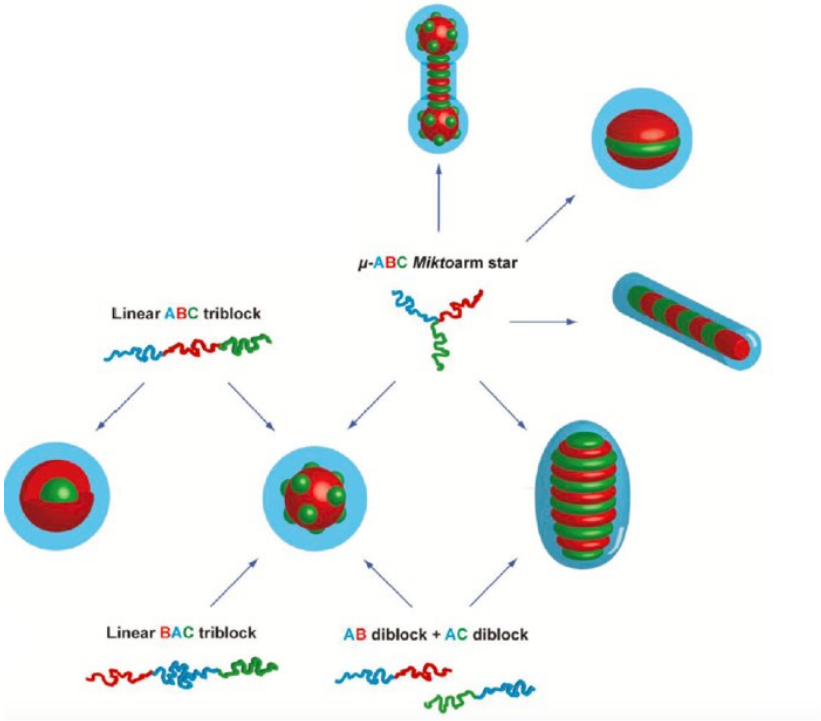

Figure 2 Schematic representation of nanostructures from linear ABC triblock terpolymer in selective solvent for **A block** with different block order: (from left) - core-shell-corona micelle with **C block** core and **B block** shell; strawberry like micelles with **B block** core and **C block** compartments. Nanostructures from *μ*-ABC Miktoarm star polymer: (from left) - strawberry-like micelle, core segmented prolate-ellipsoid micelles, (from the bottom to the top) - rod-like core-segmented particles, hamburger micelle and combination of strawberry-like micelle and core-segmented rod-like micelle.[1]

The self-assembly of BAC triblock with solvophobic B and C blocks yields the formation of core-compartmentalized micelles called raspberry like micelles. It consists of two core forming blocks B and C that are organized into separated domains. Individual compartments are in direct contact with the shell which is constituted by the A block. Another structural type which belongs to the core-shell-corona micelles is achievable by the self-assembly of ABC triblock terpolymers. Those nanostructures are

characterized by two separate interfaces that split the micelles into three spherical layers. The C block compartment does not have the direct contact with the micelle corona. In the case of the drug delivery in the inner C-core, the transported cargo needs to be released through the B domain.

2.3.2. Corona compartmentalized micelles

The self-assembly of ACB polymers forming core-corona micelles can lead also to the shell compartmentalized micelles. Such polymer can self-assemble into A-B mixed-corona system which can however undergo microphase separation by the collapse of B depending on conditions. Figure 3 is a schematic representation of the shell compartmentalized micelles.[14] The compatibility of solvophilic blocks A and B plays a crucial role in the corona architecture of linear ACB triblock terpolymers self-assembly. When the insoluble C block formed compact core is surrounded by chemically compatible A and B blocks, it concerns the mixed-corona micelles. Corona forming blocks are randomly distributed all around the core. In case of high incompatibility of A and B blocks the self-assembly yields the segregated-corona micelles or Janus particles.[10]

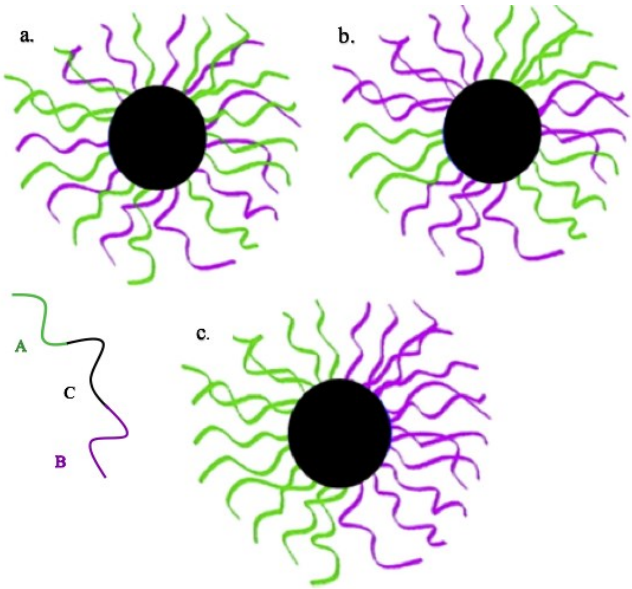

Figure 3 Schematic representation of ABC triblock terpolymer core-shell structure in selective solvent for **A block** and **B block**: (a) mixed-corona micelle, (b) segregated-corona micelle, (c) Janus particle.[11]

The major difference between those two types of architectures is the segregation level of A and B blocks. Segregated-corona micelles consist of regularly distributed clusters of individual blocks all around the C core. In case of Janus particles, A and B polymer blocks undergo the significant segregation into two separated hemi-spherical corona domains. Examples of three core-corona nanostructures are presented in Figure 3.[10,11]

2.4. Techniques for micelle-structures characterization

The self-assembly of triblock terpolymers occurs even at very low polymer concentration in aqueous solutions. These conditions can cause complications during the analysis of the micelles, and a suitable and sensitive experimental method should be chosen. Due to the high interest in nano-chemistry field and progress in physico-chemical methods, the choice of available techniques is increasing while currently used ones are still progressing. The used techniques can be distinguished considering their principles into scattering methods, spectroscopy including fluorometry and microscopy techniques such as the electron microscopy (especially cryo-TEM).

2.4.1. Light scattering

The interaction of the electric field component of light with the particle affects the electrons within the particle. It leads to an oscillating dipole and the particle becomes an emitter of the light – a scatterer.[12] The wavelength, λ, of the scattered electromagnetic wave from the particle is the same as the incident one, and it is radiated to all directions. The overall scattering of the macroscopic system is given by the summation of scattering from all components (an interference effect). In the case of homogeneous system, the scattered light is totally eliminated by destructive interference. The scattering of liquids such as pure water is caused by density fluctuations. The light scattering is important especially in the case of colloids and dispersion of nanoparticles. In such case, the spatial distribution of the scattered light reflexes the size and shape of the nanoparticle. Important parameter of light scattering measurements is the scattering angle, θ, which characterizes the angle of observation with the respect to the incident light beam. Regarding the measurement procedure of the light scattering, there are two basic approaches: dynamic and static light scattering, DLS and SLS respectively.[12,13]

The SLS technique is an optical method based on measurement of the average intensity of the scattered light as a function of the scattering angle θ in the range from 0° to 180°. The intensity of the scattered light depends on the scattering angle only for the particles larger than $\frac{\lambda}{20}$. The quantity that is used in all scattering methods is so called scattering vector $\vec{q}$. The $\vec{q}$ is defined by the difference of the wave vectors of the scattered light and the incident light $\vec{k}$ and $\overrightarrow{k_0}$ respectively

$$\vec{q} = \vec{k} - \overrightarrow{k_0} \tag{1.1}$$

For and elastic scattering process,[12,13] $q = 2a$ where $a = k \cdot sin\frac{\theta}{2}$, and $|\vec{k}| = |\overrightarrow{k_0}| = \frac{2\pi}{\lambda}$, where λ is the wavelength of the light in the particle surrounding medium. λ can be substituted by the relation of the wavelength of the incident light and the refractive index of the medium, $\frac{\lambda_0}{n}$, and therefore the amplitude of the scattering vector is:

$$q = \frac{4\pi n sin\frac{\theta}{2}}{\lambda_0} \tag{1.2}$$

For the system of analyzed particles with known concentration and refractive index increment $\frac{\mathrm{d}n}{\mathrm{d}c}$, which characterizes the contrast between the solvent and dissolved particles, it is possible to determine the weight average molecular weight M_w and the radius of gyration R_G. For the particles larger than $\frac{\lambda}{20}$, the angle-dependence of the scattering intensity leads to the form factor $P(q)$, which characterize the normalized single particle scattering of isotropic particles.[12,13] The form factor is closely related to the mass distribution within the particle and thus to its shape.

The Zimm equation

$$Kc/R = 1/M_w P(q) + 2A_2 c + \ldots \tag{1.3}$$

provides the relation between the scattered intensity of the analyzed particles, their concentration and the amplitude of the scattering vector, where R is a normalized scattered intensity (Rayleigh ratio), K is the constant that includes the square of $\frac{\mathrm{d}n}{\mathrm{d}c}$, and A_2 is a second virial coefficient which describes the interactions between the particles and solvent in term of the attractive and repulsive forces between them. By the extrapolation of the dependence of Kc/R on $P(q)$ towards the angle $\theta = 0°$ and concentration $c = 0$ g/ml, the point of the intersection of curve with the axis y is equal to $1/M_w$. The static light scattering also allows determination of another parameter which

is related with M_w such as the aggregation number, N_{agg}.[12,14] It is equal to the number of macromolecules forming the micelle. For R_G determination, the form factor is plotted against q^2. The slope of the dependence is related to R_G,[13] which is described in detail in the experimental part of the thesis.

The fundamental of DLS is based on the measurement of temporal fluctuations in the intensity of scattered light from particles that undergo random Brownian motion.[12] Detected scattered light from particles is transferred to the autocorrelation function. The difference between the principles of SLS and DLS measurements is schematically shown in Figure 4.[13]

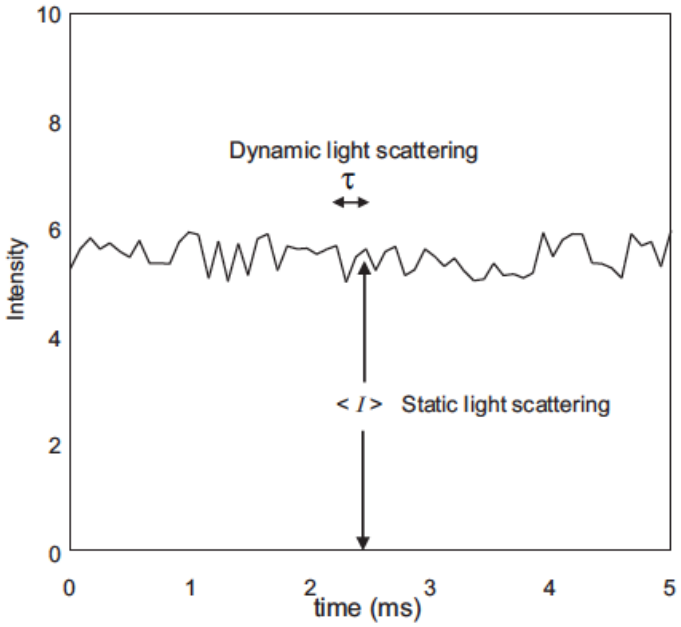

Figure 4: Fundamentals of SLS and DLS measurements.[13]

The autocorrelation function can be expressed as exponential function for the system of monodisperse spheres of radius *r*. It provides the specific correlation time, τ_{cor}, which is closely related to the diffusion coefficient of the particle, *D*. The Stokes-Einstein equation relates the diffusion and the size of the spherical particle:

$$D = \frac{k_B \cdot T}{6\pi\eta r} \tag{1.4}$$

where *T* is the absolute temperature of the suspension, η is the viscosity the liquid and k_B is the Boltzmann's constant. The apparent diffusion coefficient depends on the size or shape of the particles and the viscosity of the liquid. If particles are small, or the viscosity of the embedding liquid has a low value, particles will move more quickly

than particles of big size, in solution of high viscosity. Thus, quickly moving particles correspond to the rapidly fluctuating scattered intensity, high diffusion coefficient respectively. The experimentally found value D_{exp} can be inserted to the Stokes-Einstein equation[12] (1.4.) to solve the radius r value. The obtained radius is called the hydrodynamic radius R_H or Stokes radius, which is defined as:

$$R_H = \frac{k_B \cdot T}{6\pi\eta D_{exp}} \quad (1.5)$$

The value of particles hydrodynamic radius in solution includes also the hydration shell containing solvent molecules. Further information about multiples mathematical and physical equations used for parameters calculation is not the topic of the thesis and can be found in the literature.[12,13] The further details are shown in the experimental part of the thesis.

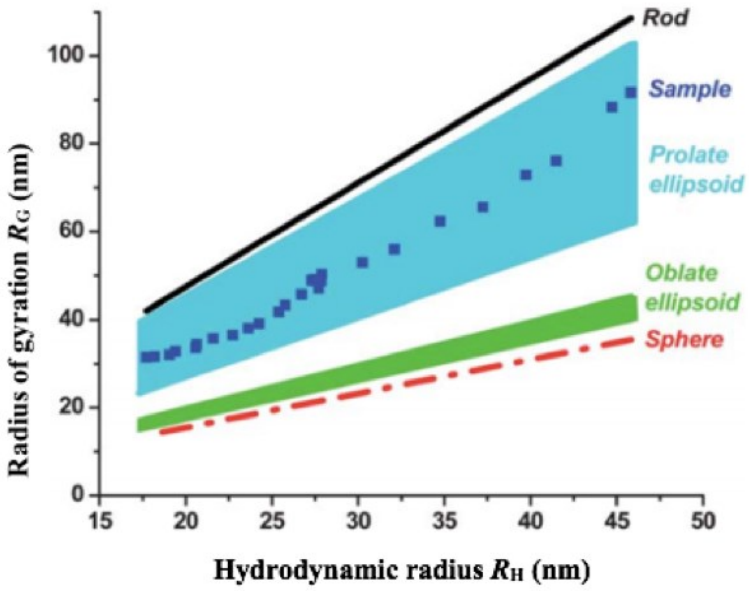

Figure 5 The theoretical prediction of silica particles shape depending on R_G and R_H values from SLS and DLS. Individual bands represent the frame of values which correspond to the possible particle architecture. Figure contain data of authors set of sample measurements, (dark blue dots) which belongs to the shape of prolate ellipsoids. [15]

Another property that can be calculated from DLS and SLS data is the shape factor of particles, R_G/R_H which provides a rough estimation of the particle shape. The shape of analyzed particles considering R_H and R_G values can vary between spheres, oblate ellipsoids through rods, which is shown in different studies.[15,16] Figure 5 is an illustrative example showing the plot of R_G against R_H with comparison of theoretical

dependences of basic shapes and experimental results obtained for silica nanoparticles in water.[15]

2.4.2. *Fluorescence spectroscopy*

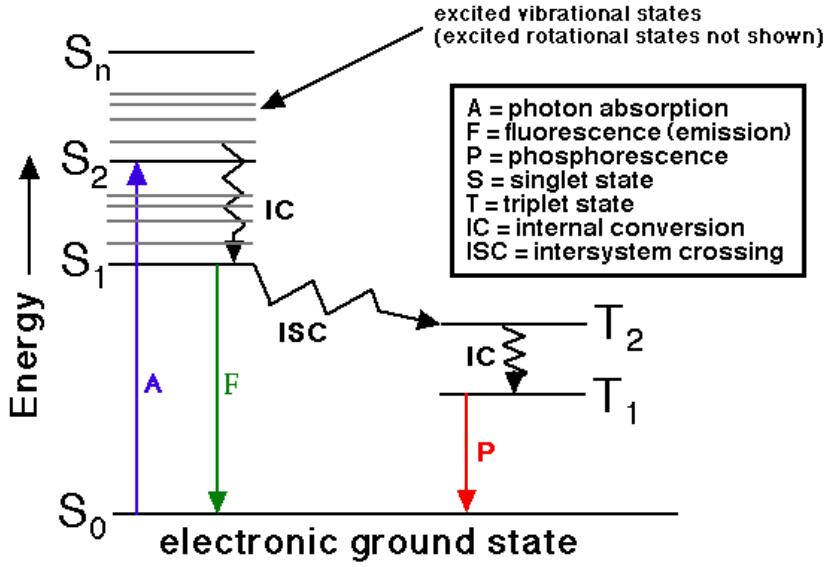

Figure 6 Jablonski diagram taken from notes of Dr. Thomas G.[20] Schematic representation of the electron transitions between the moment of its excitation until the relaxation.

The emission of light from the electronically excited states is called the luminescence. This phenomenon can be divided into two types of emission considering the nature of the excited state: fluorescence and phosphorescence.[17] After the exposure of substance to the light radiation, the substance absorbs the photon, which leads to the transition of the molecule from the ground to the excited state (S_1, S_2, etc.), see Figure 6. The emission between two states with the same spin multiplicity, called fluorescence, is allowed by selection rules and the lifetime of the excited state is usually in the range 10^{-9} to 10^{-8} seconds. Another type of the excitation energy dissipation within two states with the same spin multiplicity is called the internal conversion.[17,18] It is a nonradiative process. The internal conversion occurs very fast, from 10^{-14} to 10^{-11} seconds in between electronic levels higher than the S_1, for example between S_1 and S_2. If the spin multiplicity changes, for example from the first excited singlet state S_1 to the first excited triplet state T_1, it concerns the intersystem crossing. Very slow intersystem crossing can be followed by the emission from the first excited triplet state T_1 to the

ground state S_0 with the lifetime from milliseconds to seconds, called phosphorescence.[17,18,19] The process between the absorption of light and its emission related to the electron transition is usually described by Jablonski Diagram, Figure 6.[20]

Substances capable to emit light after being excited are called fluorophores. Those are typically aromatic compounds as for example pyrene, anthracene or coumarin. The average time of electron transition to the ground state varies within the diversity of fluorophores and is called the fluorescence lifetime τ. Fluorescence emission is sensitive to surrounding solution conditions and the vicinity of fluorophore with any substances able to absorb or quench the emission of studied fluorophore[17]. Sensitivity of lifetimes to different solutions and environments allows studying the inner structure of the nanoparticles. This phenomenon is used in the thesis to study fluorophores solubilization in micelles.[17,18,19]

The fluorescence spectra are usually presented as the dependence of the fluorescence intensity on the wavelength. Two types of spectra are used: emission and excitation spectra. The plot of fluorescence intensities against varying emission wavelengths while the excitation wavelength is kept constant is called emission spectra. When the excitation wavelength varies while the emission wavelength is kept constant, the resulting spectrum is the excitation spectrum.[17] Generally, it is possible to conclude that the emission spectra serve to determine wavelengths at which the molecule efficiently emits fluorescence. The excitation spectra are used to determine the wavelength with the efficient absorption of light that is capable to induce the emission. Both spectra types are useful to study an impact of different environments on spectral characteristics of the probe. Alternatively, it can be also used to analyze the fluorescence quenching and the energy transfer between fluorescence probes. The interpretation of lifetime and emission spectra are further described in the experimental part.[17,18,19]

The method of fluorescence resonance emission transfer,[17,18] FRET, concerns a process of energy transfer from the first excited singlet state of the donor to the first excited singlet state of the acceptor. It is a non-radiative transfer which is not mediated by photon, but which occurs through the dipole-dipole interaction between the donor and the acceptor at their distance under 10 nm without a mutual collision. The distance at which the transfer occurs at 50% effectiveness is called the Förster radius. Study of this phenomenon provides information about the structure of block copolymer micelles and their compartments of various microenvironments.[19]

2.4.3. Cryogenic transmission-electron microscopy

The development of cryogenic electron microscopy abbreviated as cryo-EM became a mainstream technology thanks to its wide range of use in structural characterization. The cryo-EM gives possibility to image intact tissues, molecular morphologies, viruses, protein molecules and many other structures.[21] This technique includes multiple sub-categories considering the principle of electron microscope measurement such as cryogenic transmission electron microscopy, (cryo-TEM) and cryogenic scanning electron microscopy, (cryo-SEM).

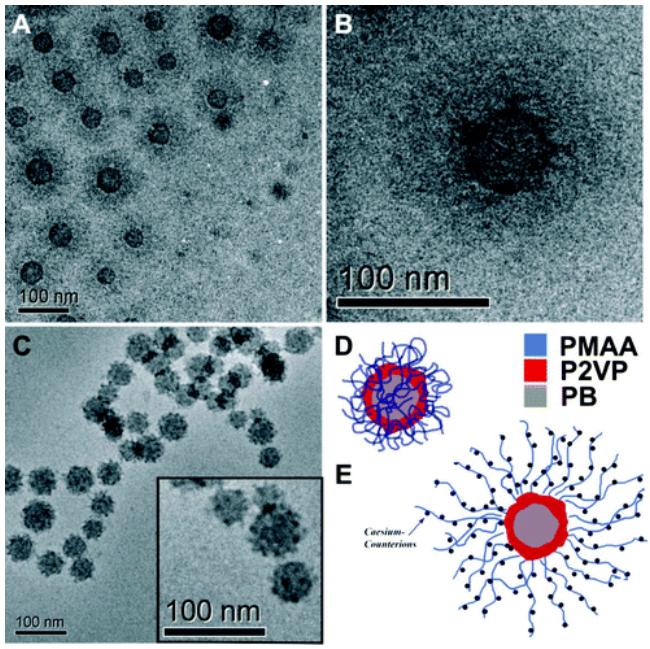

Figure 7 Cryo-TEM micrographs of $PB_{800}P2VP_{190}PMAA_{550}$ in aqueous solution at pH 10 (0.05 M CsCl, c = 1 g/L), Overview (A) and single core−shell−corona micelle (B); at pH 4 (c = 1 g/L) (C), the inset shows an enlargement; schematic depiction of the proposed solution structure of $PB_{800}P2VP_{190}PMAA_{550}$ depending on the pH; core−shell−corona structure with an expanded PMAA corona at pH 10 (E) and micelles with a collapsed PMAA corona at pH 4 (D).[23]

The fundamental of the cryo-TEM approach is to study a thin amorphous ice layer of radiation-sensitive samples at cryogenic temperature. It is a method that provides direct imaging of the sample without perturbing nanoparticles, for example by deposition on the substrate in the dried state. The technique of transmission electron microscope is based on somehow similar principles as the classical light microscope, which is not suitable for visualization of nanoparticles due to the diffraction limit. Electron microscopy, especially cryo-TEM, provides high-resolution images giving possibility to determine the size of nanoparticles in solution and eventually to distinct

the subdivided domains of multicompartment nanoparticles.[22] A typical example of micellar morphology visualization by cryo-TEM micrographs is shown in Figure 7.[23]

2.5. Application of multicompartment micelles

The range of application for well-defined multicompartment nanoparticle is rapidly increasing, especially in medicine. Nanoparticles find application in treatment of cardiovascular disease and diabetes, but the main part of research is oriented towards the cancer treatment. The multicompartment nanoparticles are the promising candidates for drug delivery, imaging and other advanced techniques.[24,25, 26]

2.5.1. Drug delivery

Nanoparticles find potential in medical applications thanks to their characteristics that shows better impact than classical medication treatment. Classical free drugs fail on the drug dosage accompanied by significant side-effects. The general advantage of nanoparticle drug delivery lies firstly on hydrophobic drug encapsulation that restrains the medication effect on healthy cells. The multicompartment nanoparticles are advantageous in ability of double delivery that allows to encapsulate and to transport two incompatible drugs with dosage much higher than for free drugs. Loaded nanostructures are distributed through the blood circulation within human body in way to reach the cancer tissues where the transferred cargo is released. Intravenously administered nano-sized drugs benefit from longer period of circulation in blood thorough their size which is big enough to avoid the excretion by kidneys and small enough to be prevented from the recognition by reticuloendothelial system. For reaching the tumor tissues, the nanoparticles containing the cargo are distributed by passive or active transport, which is in many cases the combination of both.[24,26]

The passive transport of nanoparticles characterizes their retention in tumorous tissues from the blood flow. The neovascularization in the near area of tumors enhance the blood flow towards them in way to provide all nutrients needed for fast growth. Thus, the larger proportion of nano sized drugs from blood circulation can reach the cancerous tissues in comparison with healthy one. In return tumors are lacking the lymphatic drainage that ensures the gathering of nanoparticles inside them. That effect

of passive accumulation of macromolecules in tumors is called the enhanced permeability and retention effect, (EPR).[27, 28, 29, 30]

The active transport does not rely on the accumulation in tumors through the blood flow but can ensure the target transport through to the benefits from the nanoparticles polymer properties. Nanoparticles can be composed from pH responsive substances, blocks in case of block copolymer micelles. The pH in proximity of cancerous tissues is more acidic (pH ≈ 5.0 – 6.5) than in healthy tissues (pH ≈ 7.2 – 7.4).[28] Thus, the macromolecule can be cleft by the enzymes in hypoxic surrounding of tumor in way to release the drug. Alternatively, receptor mediated endocytosis of micelles can be applied to ensure the specificity towards the tumor and drug targeting. The modification of nanoparticles by transferrin is frequently applied due to the elevated number of transferrin receptors on the tumor surface. In way to enhance the effectivity of drug delivery, specially modified nanoparticles that undergo the EPR are used as a combination of active and passive transport.[24,27, 28]

2.5.2. Boron neutron capture therapy

The progress in the field of radiotherapy is mainly marked by the selective treatment by neutron capture therapy based on non-radioactive isotopes use as for example boron and gadolinium. That noninvasive method finds primary use for malignant brain tumors treatment and can be also applied in recurrent head and neck cancer treatment. It concerns two steps procedure characterized at first by the localization of tumor by injected localizing drugs containing non-radioactive isotope of boron (^{10}B). Boron-10 is then irradiated with epithermal neutron source that provokes the biologically destructive nuclear capture reaction with boron-11 as a product which eases the nuclear fission by forming the α particle (^{4}He), and high energy lithium nucleus (^{7}Li). Both the lithium ions and alpha particles produce ionizations in the boron containing cancerous cells which are sufficiently lethal for tumor cells. Targeted delivery of boron-10 compounds to the tumor tissues limits the effect of nuclear fission reaction on normal, healthy tissues. The efficacy of BNCT method is based on elevated intercellular concentration of boron-10 that is possible to reach by the way of well-defined multicompartment nanoparticles administration.[31, 32]

3. Aims of the thesis

This thesis is a contribution to the study of amphiphilic triblock terpolymer and diblock copolymer micelles in the Soft Matter group, Department of Physical and Macromolecular Chemistry. The aims of this bachelor thesis are following:

1. To prepare, in a controlled manner, micellar solutions of amphiphilic poly(acrylic acid)-*b*-poly(4-hydroxystyrene)-*b*-poly(styrene-carborane) triblock terpolymer and of related poly(acrylic acid)-*b*-poly(4-hydroxystyrene) diblock copolymer.
2. To characterize prepared micelles in aqueous solution in terms of size, shape and molar mass.
3. To study the solubilization of model drugs (2-methylnaphtalene and 7-methoxycoumarin-carborane fluorophores) in nanoassemblies by means of fluorescence spectroscopy.

The obtained knowledge will allow for a reproducible preparation of stable multicompartment amphiphilic boron-containing nanoparticles in aqueous solution and for the understanding of the influence of preparation protocol on self-assembly behavior of block copolymers.

4. Materials and used methods

4.1. Used polymer samples and chemical substances

Both poly(acrylic acid)-*b*-poly(4-hydroxystyrene)-*b*-poly(styrene-carborane), PAA-*b*-PHS-*b*-PSC, triblock terpolymer and related poly(acrylic acid)-*b*-poly(4-hydroxystyrene), PAA-*b*-PHS, diblock copolymer were synthesized in cooperation with Dr. Krzysztof Rodzeń and Dr. Adam Strachota, IMC, The Czech Academy of Sciences. Both were prepared via RAFT polymerization and post-polymerization modification (hydrolysis) reaction.

For the solvent mixtures for the polymers dissolution the following solvents were used: the tetrahydrofuran (THF), (anhydrous ≥ 99.9%, inhibitor free, Sigma-Aldrich, USA), phosphate buffered saline (PBS), (tablet, Sigma-Aldrich, USA) and deionized water prepared by reverse osmosis.

Fluorescence studies were carried out with two fluorophores: 2-methyl naphthalene (97%, Sigma-Aldrich, USA), and coumarin-carborane based probe, (CBMC) prepared by Jiří Schimer (group of Petr Cígler, IOCB, The Czech Academy of Sciences); Structures in Figure 8.

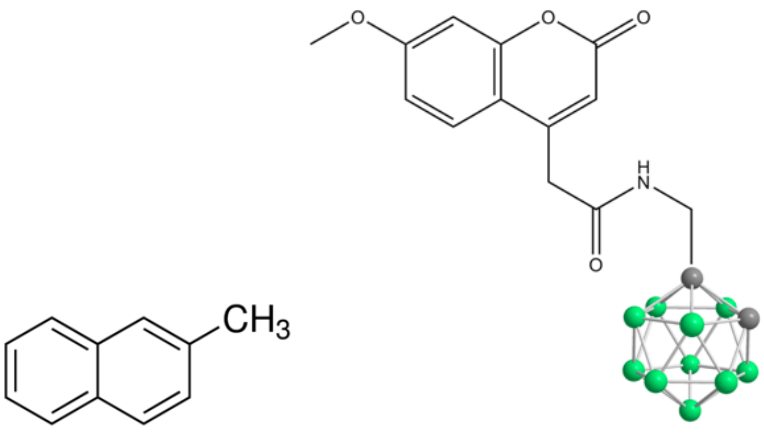

Figure 8 The fluorophores: 2-methylnaphthalene, N, (left), and 7-methoxycoumarin-carborane conjugate, CBMC, (right).

4.2. Micelles preparation in solvent mixtures

PAA-*b*-PHS-*b*-PSC triblock terpolymer and PAA-*b*-PHS diblock copolymer micelles were prepared in THF-PBS or THF-H_2O solution mixtures. THF was used as a selective solvent for PHS and PSC blocks. The micelles preparation was organized in set of three different experiments. *Experiment 1* and *experiment 2* (described below) were carried out to understand the behavior of polymers in THF-PBS and THF-H_2O solution mixtures with various solvent fractions. E*xperiment 3* was centered on the study of the self-assembly behavior of the polymers.

Two micellization methods were used to obtain nanoparticles. On the one hand, water was poured drop-wise into the organic phase (solvent mixture with dissolved polymer) at constant rate and under vigorous stirring; this was termed "titration method". On other hand, the organic phase was poured drop-wise into water at constant rate and under vigorous stirring; this was termed "quenching method". After the *experiment 2*, the quenching method was found to provide nanoparticles of better quality. Thus, it was used for the rest of experiments.

Experiment 1- Preparation of PAA-*b*-PHS-*b*-PSC *and* PAA-*b*-PHS *nanoparticles in solvent mixtures* THF-PBS:

Tetrahydrofuran was used as the initial solvent for each polymer. 2 ml of THF were introduced into two distinct vials containing each approximately 20 mg of PAA-*b*-PHS and PAA-*b*-PHS-*b*-PSC. Samples were stirred for one hour and subsequently heated for 20 minutes at 40°C, but PAA-*b*-PHS was not dissolved. For further dissolution, 0.5 ml of PBS was added to both polymer solutions. After another hour of agitation, triblock terpolymer was completely dissolved. The diblock copolymer was dissolved, but the solution appeared milky. The organic phase (dissolved polymers, each in 2.5 ml of THF-PBS mixture) was titrated by 7.5 ml of PBS. The droplet rate of titration was 0.5 ml/min. The formation of micelles was expected due to the kinetic "freezing" of nanoparticles upon addition of the buffer (good solvent for PAA block). Total volume of solution was 10 ml with concentrations of 2.60 mg/ml for PAA-*b*-PHS and 2.02 mg/ml for PAA-*b*-PHS-*b*-PSC.

2 ml of each sample was used for DLS and SLS analysis. The measurements were carried out at different angles (30°-150°, with 5° step). The R_H^{app} values were calculated. Small volume of each sample (≈ 0.2 ml) was used for Cryo-TEM analysis.

After several days the polymer solutions partially precipitated what ruled out further analysis. Used PBS buffer was than substituted by deionized water which was used for the rest of the studies.

Experiment 2 - Preparation of PAA-*b*-PHS-*b*-PSC *nanoparticles in different solution mixtures of* THF- H_2O:
Various solvent mixtures of THF-H_2O, ranging from 10% to 90% v/v THF, were prepared. In a typical experiment 2 mg of PAA-*b*-PHS-*b*-PSC were weighted and dissolved in 2 ml of the chosen solvent mixture. Samples were stirred for 24 h to ensure complete dissolution of polymer. Used vials were cleaned with acetone and dried. THF and H_2O were filtered by 0.2 μm membrane filters to eliminate the dust in solutions.
Light scattering measurements of each sample were carried out at different angles (30°-150°, with a 10° step). Obtained data was used to calculate R_H^{app}.

Experiment 3 - Preparation of PAA-*b*-PHS-*b*-PSC *nanoparticles in water solution.*
Vials were cleaned and solutions of THF and H_2O handled as described in *experiment 2.* Based on results from the previous experiment three solvent mixtures were selected (10%THF, 50%THF and 90%THF) for preparation of the nanoparticles.

In a typical experiment 2 mg of PAA-*b*-PHS-*b*-PSC were dissolved in 2 ml of each solvent mixture noted and stirred until complete dissolution. This solution was then poured drop-wise into 2 ml of water. The addition rate was kept constant to ensure reproducibility (0.5 ml/min). Quenched solutions were dialyzed several times against deionized water to remove traces of THF and switch the solvent mixture to a PAA selective solvent. Final concentrations were recalculated after dialysis due to changes in volume.

DLS and SLS were measured for all the samples at different angles (30°-150°, with 10°step). Data obtained was used to determine R_H^{app} and R_G values. Steady-state and time-resolved fluorescence studies were carried out for these samples as described

below. A small volume of each sample (≈ 0.2 ml) was used for Cryo-TEM analysis. This method was found as suitable for the preparation of well-defined micelles with long stability time and was used for the rest of the PAA-*b*-PHS-*b*-PSC study analyzed in this thesis.

4.3. Dynamic and static light scattering

The light scattering measurements (DLS and SLS) were performed with the He-Ne laser (λ = 632.8 nm), an ALV CGS/8F goniometer, an ALV High QE APD detector and an ALV 5004 multibit, multitau autocorrelator, (ALV, Langen, Germany). The samples were filtered during the preparation through 0.2 μm membrane filter, measured in cleaned vials at 25°C for the scattering angles ranging from 30° to 150°, with an angular step of 5° or 10°. The SLS data were treated by standard Zimm method. The DLS analysis was performed by the ALV software based on CONTIN algorithm.

4.4. Fluorescence spectroscopy

Fluorescence emission measurements were carried out in 1 cm quartz cuvettes using a Fluorolog FL 3-22 fluorometer (Horiba Jobin Yvon, France) equipped with double-grating excitation and emission monochromators, a FluoroHub time-correlated single photon counting module and a TBX single photon counting detector. Steady-state fluorescence measurements were performed using a 450 W high-pressure xenon arc lamp as a light source. Fluorescence emission decays were measured using NanoLed diode laser sources of appropriate wavelength, operated at the repetition frequency of 1 MHz. The decays were fitted by using a Horiba DAS6 software performing the iterative reconvolution of the fitted model with the instrument response function by means of the Marquardt-Levenberg least squares algorithm.

4.5. Cryo-TEM

The Cryo-TEM measurements were performed by Dr. Sami Kereïche from Institute of Cellular Biology and Pathology, First Faculty of Medicine, Charles University, Prague. A volume of 3 μl of the sample solution was applied to an electron microscopy grid

with carbon-covered polymer supporting a film (lacey-carbon girds LC200-CuC, Electron Microscopy Sciences), glow discharged for 40 s with a 5 mA current. The grid was immediately plunged into liquid ethane held at -183°C. The sample was then transferred without re-warming into a Technical Sphera G20 electron microscope (FEI, Hillsboro, OR). Images were recorded 120 kV accelerating voltage and microscope magnifications ranging from 5000x to 14500x using a Gatan UltraScan 1000 slow scan CCD camera.

5. Results and discussion

5.1. Polymer synthesis

Poly(*tert*-butyl acrylate) was synthesized as the first block of the future copolymers (see Figure 9). AIBN was employed as radical initiator and the trithiocarbonate compound as chain transfer agent (CTA). Toluene was used as solvent to avoid an excessive increase in viscosity during the polymerization, which resulted in relatively high monomer conversions achieved without precipitation. The product **1** (P*t*BA) was used (after removal of monomer residues) as macrotrasfer agent for chain extension with 4-acetoxystyrene. This latter reaction also was conducted in toluene, as the starting compound was a solid. It was carried out overnight and yielded the diblock copolymer **2**. After the isolation a portion of **2** was used to produce the triblock terpolymer (**3)** by reaction with the styrene-carborane (SC) monomer.

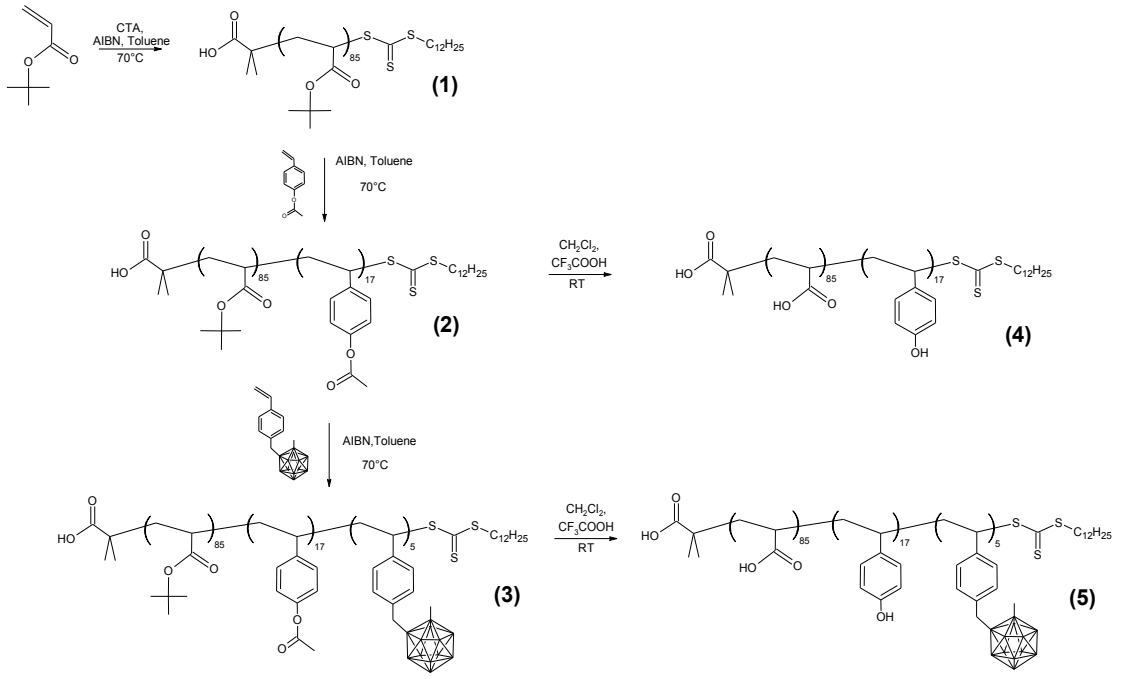

Figure 9 Synthetic routes used for preparation of (**5**) PAA-*b*-PHS-*b*-PSC and (**4**) PAA-*b*-PHS.

This monomer was prepared by the group of prof. Rosario Núñez (ICMAB, Barcelona) and its synthesis was described in reference 33. The below-discussed results indicate a fairly high efficiency of the used RAFT initiating system for this monomer. Finally, the product **3** was subjected to the acidolysis of the pendant ester groups in the poly(*t*BA) and poly(AOS) blocks, which yielded poly(acrylic acid)- and poly(4-

hydroxystyrene)-blocks respectively in the final product. The reaction was carried out in dichloromethane, using trifluoroacetic acid as the acidolysis agent. The amphiphilic triblock terpolymer **5** was thus obtained as final product and was purified by dialysis. As a reference system, the boron-free diblock copolymer **2** also was converted by acidolysis into the diblock copolymer **4**, in a fully analogous way like the **3** → **5** acidolysis.

The final products of each synthesis step were analyzed by ^{1}H NMR and SEC, in order to verify their structure and purity, and to determine their molecular mass (see Table 1). The comparison of M_n of values obtained by SEC and ^{1}H NMR indicates different values, in way that SEC values are based on mass calibration with polystyrene standards, while the values obtained from ^{1}H NMR spectra are based on true ratios of structural units.

Table 1 Molecular weights and dispersities of the prepared polymers, as determined by SEC and ^{1}H NMR spectroscopy; ratios monomer/chain-transfer-agent/initiator are also listed. [a][M]/[CTA]/[I] eq. of monomer, chain transfer agent or macrotransfer agent and initiator; [b]Measured by SEC calibrated with PS standards in THF as eluent; [c]Determined by ^{1}H NMR spectroscopy.

Code	Polymer[c]	[M]/[CTA]/[I][a]	M_n (SEC)[b] Da	M_w (SEC)[b] Da	M_w/M_n (SEC)[b]	M_n (^{1}H NMR)[c] Da
1	P*t*BA$_{85}$	200/1/0.2	18001	20548	1.11	11259
2	P*t*BA$_{85}$-*b*-PAOS$_{17}$	100/1/0.3	22177	28711	1.29	14016
3	P*t*BA$_{85}$-*b*-PAOS$_{17}$-*b*-PSC$_5$	50/1/0.5	21173	31066	1.46	15383
4	PAA$_{85}$-*b*-PHS$_{17}$	-	-	-	-	8532
5	PAA$_{85}$-*b*-PHS$_{17}$-*b*-PSC$_5$	-	-	-	-	9899

5.2. Micelle characterization

The solubility of PAA-*b*-PHS-*b*-PSC and PAA-*b*-PHS was studied in THF-PBS and THF-H_2O solvent mixtures. Micellar solutions of triblock and diblock were prepared by controlled polymer dissolution in THF-H_2O solvent mixtures. The micellar size and shape was characterized by DLS and Cryo-TEM.

PAA-*b*-PHS-*b*-PSC and PAA-*b*-PHS were initially dissolved in THF-PBS solution mixture. The polymers underwent only a very slow dissolution and required several hours of stirring and heating at 40 °C. This choice of solvents did not provide well-defined samples in term of polymer solubility. The salt effect of the used buffer in solution mixture did not offer suitable conditions for polymer stability and caused its precipitation within several days after the polymer dissolution. As a subsequent experiment, PAA-*b*-PHS-*b*-PSC solubility was studied by various THF-H_2O mixtures with different composition, ranging from 10%THF to 90%THF. The solubility of the polymer improved with the increasing THF content in solvent mixture. Solvent mixtures containing from 10% to 30% of THF underwent slow dissolution (several hours), solvent mixtures of higher THF volume fraction readily dissolved the polymer. The series of polymeric solutions of samples with 10%, 20%, 30% and 50% THF shown significant scattering of light to the naked eye, early indication that the self-assembly was successful. No signs of polymer precipitation were observed therefore the THF-H_2O solvent mixtures were a suitable choice of initial solvents for PAA-*b*-PHS-*b*-PSC and PAA-*b*-PHS samples.

Individual solution mixtures with different THF-H_2O content were characterized by light scattering measurements to analyze the effect of the solvent on micellar size and shape, (Figure 10). The micellar size of samples with 60-90% THF content markedly increases. This effect is caused by highly swollen PSC and PHS blocks by THF inside of the micellar core. When the THF volume ratio is in minority, from 20% to 40%, micellar size decreases. In that situation the volume of THF in micellar core-shell area is small, and that PSC and PHS blocks are less swollen. The micellar size in those solutions is influenced also by the polyelectrolyte effect of PAA block. When the volume fraction of both solvents is equal, e.g. 50% of THF and 50% of H_2O, there is an interesting drift of micellar size in comparison with the continuous curve evolution. This unexpected behavior was observed by naked eye, when the micellar solution highly scattered light. The dependence of R_H^{app} in various THF volume fractions was also manifested in CONTIN distributions (Figure 10), (constrained inverse Laplace transform routine). It is the distribution of apparent hydrodynamic radii at the scattering angle $\theta = 90°$ for each solution mixture sample.

As a subsequent experiment, *experiment 3,* three types of solvent mixtures from the THF-H_2O series of polymer solutions were chosen for further studies. PAA-*b*-PHS-*b*-PSC triblock terpolymer was dissolved in THF-H_2O mixtures containing 10%, 50%

and 90% of THF and PAA-*b*-PHS was dissolved in mixture containing 90% of THF. After that, water content was increased to achieve the kinetically frozen particles. The rest of THF was removed by dialysis against water. The new PAA-*b*-PHS-*b*-PSC and PAA-*b*-PHS nanoparticles in water were analyzed by the dynamic light scattering. The obtained R_H^{app} values were compared with the R_H^{app} values of nanoparticles in THF-H_2O solvent mixtures (*experiment 2*).

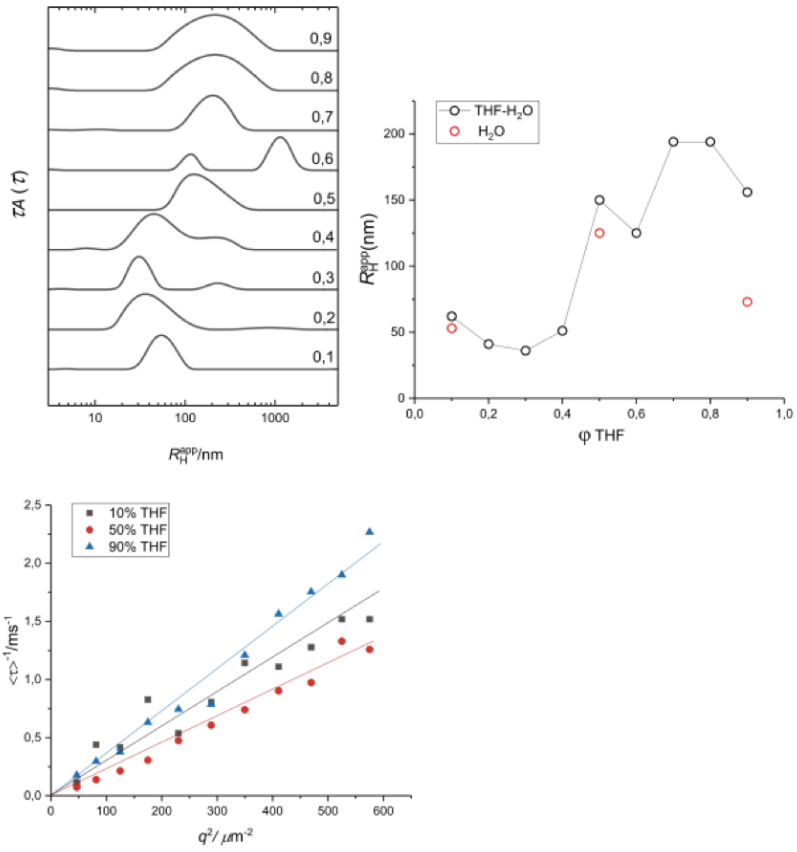

Figure 10 (left, top) CONTIN analysis – the size distribution of PAA-*b*-PHS-*b*-PSC at scattering angle θ = 90° for different initial THF-H_2O mixture composition: 10% of THF correspond to the curve 0.1; 20% of THF corresponds to the curve 0.2 etc. (right) – Dependence of R_H^{app} on THF fraction in THF-H_2O mixture before the dialysis against water – black circles, and after dialysis – red circles. (left, bottom) the relaxation rates $1/\tau$ as a function of q^2 for the samples of triblock from solvent mixture with 10%, 50% and 90% of THF content.

The difference between the R_H^{app} values (Figure 10) is more evident with increasing THF content in initial solvent mixture. The lowest content of THF produced only small swelling of micellar core and its removal during dialysis did not cause any substantial change in the compactness of the micellar core. Higher amount of THF in solvent mixtures, 50% and 90% of THF, resulted in high core swelling, and the removal of THF by dialysis against water caused an observable size reduction due to the collapse of core forming blocks in presence of non-solvent. To summarize the effect of solvent change

by dialysis on R_H^{app} values, increasing amount of THF cause increasing core swelling during micelle formation thus, higher the core swelling is, more intense the size reduction after the THF elimination from solution is observable.

Figure 10 shows also the dependence of correlation rates $1/\tau$ as a function of q^2 for the samples PAA-*b*-PHS-*b*-PSC with initial solvent mixture containing 10%, 50% and 90% of THF. The linear dependence with the origin in zero shows that the DLS correlations of the nanoparticles correspond to the fluctuations of the particles due to the Brownian motion. The linear fit of the sample from initial solvent mixture containing 10% of THF leads to a significant deviation from the linearity which indicates the presence of additional relaxation processes or "higher modes", as expected for rod-like particles at higher q.[12]

Multiple times prepared micelles shown the reproducibility of chosen preparation steps including kinetical freezing by quenching and dialysis against water. Relatively stable R_H^{app} values for PAA-*b*-PHS-*b*-PSC and PAA-*b*-PHS nanoparticles in aqueous solutions reproduced multiple times were detected by DLS analysis, and the solutions stability was observed for longer than one year.

The shape of micellar structures of solutions with 10%, 50% and 90% of THF for triblock and 90% of THF for diblock were studied by the $\frac{R_G}{R_H}$ ratio and cryo-TEM micrographs. The R_G values were obtained from the Zimm method from SLS measurements (see Review of the literature and equation (1.3)). The R_G and R_H^{app} are shown in Table 2 where can be also found the theoretically calculated shapes of the nanoparticles as reported in reference 12 (for comparison see cryo-TEM micrographs below).

Static light scattering analysis permits to obtain mass-weighted average molecular weight of the micelles, M_w, which allows the calculation of the aggregation number, N_{agg}. For the M_w determination it was necessary to know refractive index increment and solution concentration. The value of $\frac{dn}{dc}$ was calculated from the following relation

$$\frac{\mathrm{d}n}{\mathrm{d}c} = \frac{\mathrm{d}n}{\mathrm{d}c}(\mathrm{PAA}) \cdot w_{\mathrm{PAA}} + \frac{\mathrm{d}n}{\mathrm{d}c}(\mathrm{PHS}) \cdot w_{\mathrm{PHS}} + \frac{\mathrm{d}n}{\mathrm{d}c}(\mathrm{PSC}) \cdot w_{\mathrm{PSC}} \qquad (1.6)$$

where $\frac{dn}{dc}$ stands for refractive index of an individual block and *w* refers to the weight fraction of an individual block. Due to the short length of the PSC block in PAA-*b*-PHS-*b*-PSC, same $\frac{dn}{dc}$ values for diblock copolymer and triblock terpolymer were used for the calculations with the resulting value of $\frac{dn}{dc}$ = 0.175 · 10^{-3} ml/g. M_w^{app} of the micelles was obtained from the corresponding partial Zimm plots. The extrapolation of the Kc/R dependence on $P(q)$ towards the angle θ = 0° and concentration c = 0 g/ml was realized partially, with only one concentration of analyzed samples. Thus, the molecular weight was named apparent and not absolute. The N_{agg} was calculated by dividing the micellar concentration by the weight of the corresponding polymer. N_{agg} was used for calculation of micellar concentration, $c_{micellar}$, from molar concentration of polymer divided by N_{agg}. The M_w^{app}, N_{agg} and $c_{micellar}$ values for individual samples are included in Table 2.

Table 2 Shape factor of particles, SLS and DLS results for ABC triblock terpolymer (Tri) and AB diblock copolymer (Di) in THF-H_2O mixtures; Predicted shape[15] – Pr.S; Obtained shape by cryo-TEM – Ob.S; Abbreviations for nanostructures shape: W – worm, S – sphere, P – prolate ellipsoid; mass weighted molecular weight – M_w^{app}; aggregation number – N_{agg}; micellar concentration – c_{mic}.

Polymer/ solvent composition	R_G **[nm]**	R_H^{app} **[nm]**	R_g / R_H^{app}	**Pr.S.**[15]	**Ob.S.**	$M_w^{app}\cdot10^8$ **[g/mol]**	N_{agg} $\cdot10^2$	$c_{mic}10^{-10}$ **[mol/l]**
Tri 10%THF	105	47	2.23	W	W	1.69	170	0.28
Tri 50% THF	101	125	0.81	S	S	6.90	7000	5.70
Tri 90% THF	96	73	1.51	P	P, W	0.550	56	0.73
Di 90% THF	117	130	0.9	S	S	0.717	840	5.00

The shape factor $\frac{R_G}{R_H}$ values serve only as approximate information about nanoparticles shape. The direct method for determination of micellar shape and morphology is cryo-TEM, which however confirmed the shape estimated by SLS and DLS measurements. Micrographs for each sample are presented, starting with PAA-*b*-PHS-*b*-PSC sample from initial solvent mixture containing 10% of THF in THF-H_2O mixtures, which correspond to wormlike micelles, (see Figure 11) as calculated from the shape factor.

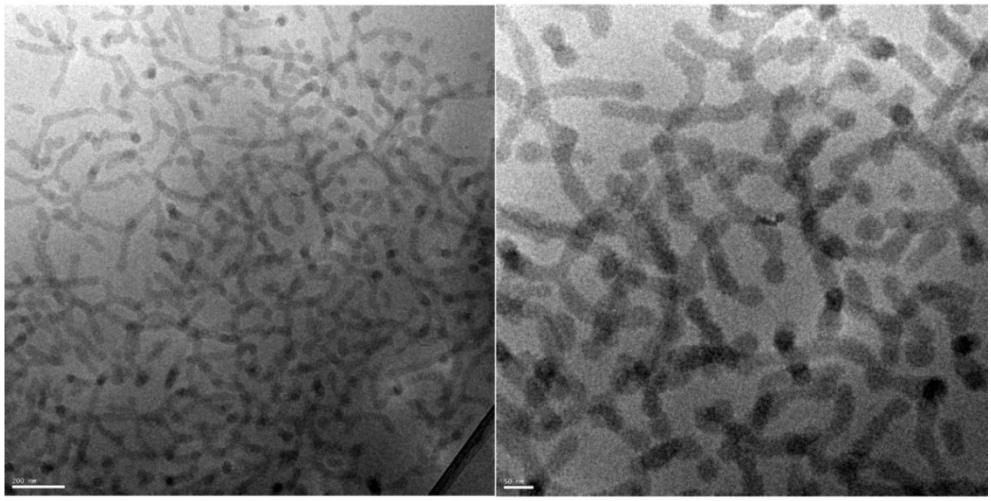

Figure 11 Cryo-TEM of wormlike PAA-*b*-PHS-*b*-PSC micelles from initial solvent mixture THF-H_2O with 10% of THF: Scale bar (left image) – 200 nm, (right image) – 50 nm.

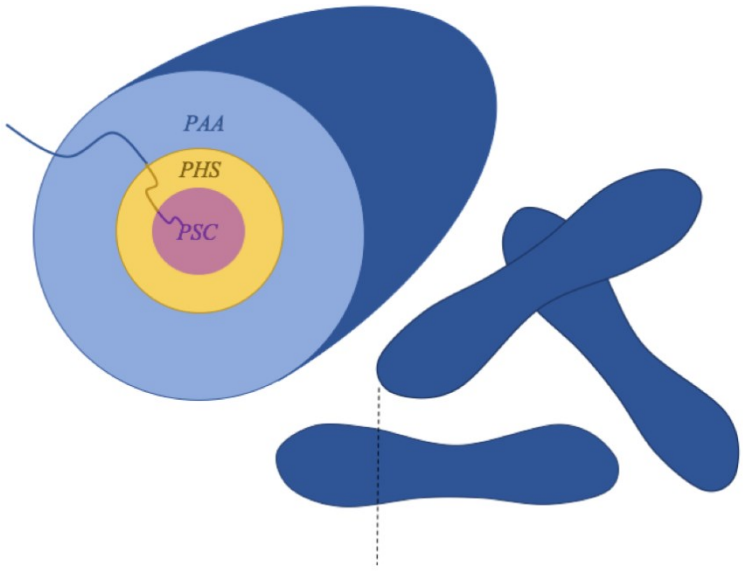

Figure 12 Visualization of wormlike core-shell-corona PAA-b-PHS-b-PSC micelle; **PSC** core, PHS shell, **PAA** corona.

Cryo-TEM micrographs did not directly confirm the presence of compartments created by different blocks in the terpolymer. The higher contrast of individual compartments could be obtained by addition of metal-oxide to the micellar solution. Its bonding with one particular polymer block would enhance the electron density by adding a contrast element to the picture. Darker areas observed in worm-like micelles are created by the superposition of individual particles. The short length of the third polymer block, PSC, could be another reason why the microphase separation within the core of the

nanostructures is not observed. The expected wormlike particles with small sized core and shell, surrounded by large corona are shown in Figure 12.

Significantly smaller number of spherical micelles is observed in cryo-TEM micrographs of PAA-*b*-PHS-*b*-PSC sample from initial THF-H_2O solvent mixture with 50% THF content (see Figure 13).

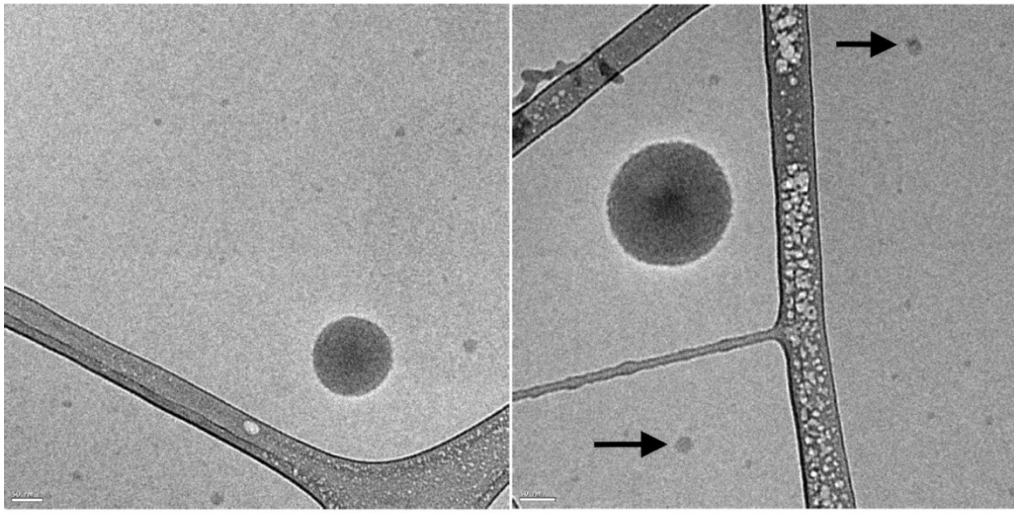

Figure 13 Cryo-TEM of spherical PAA-*b*-PHS-*b*-PSC micelles from initial solvent mixture THF-H_2O with 50% of THF: Scale bar – 50 nm.

The lower number of particles is explained by a high increase in aggregation number. This enormous gain in number of polymer chain per micelle leads to the formation of micelles with larger hydrodynamic radii. The spherical shape calculated from the shape factor was confirmed by a few particles with radius corresponding approximately to R_G values, found in cryo-TEM micrograph. Several small particles of small size (marked by an arrow) were found in analyzed micellar solution, but the main point of interest was in bigger nanoparticles with core-shell-corona structure. More compact core with contrasted central parts than in case of previous sample was observed. The expected micellar organization of core-shell-corona structure is represented in Figure 14.

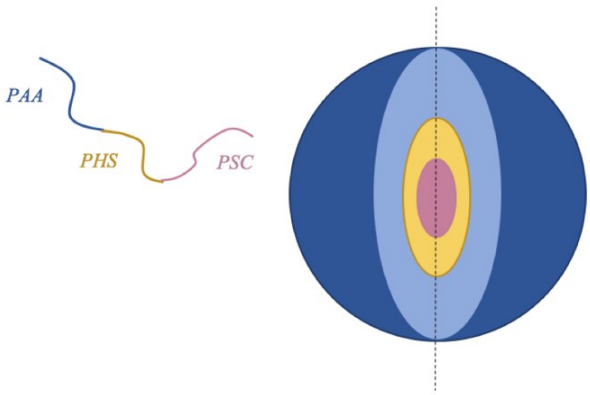

Figure 14 Visualization of spherical core-shell-corona PAA-*b*-PHS-*b*-PSC micelle: **PSC** core, PHS shell, **PAA** corona.

The calculated shape of prolate ellipsoid for PAA-*b*-PHS-*b*-PSC sample from initial solvent with 90% THF content in initial THF-H_2O solution mixture was also confirmed by cryo-TEM, but also unforeseen wormlike particles were present in analyzed solution, (see Figure 15). Compartments were not observed for the same reason of low contrast as for previous samples.

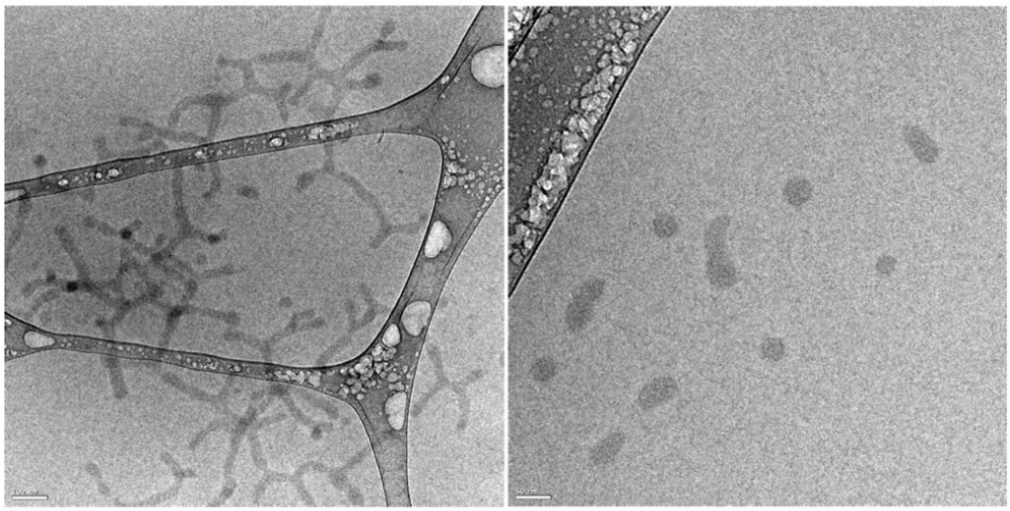

Figure 15 Cryo-TEM of spherical PAA-*b*-PHS-*b*-PSC micelles and prolate ellipsoids/worms from initial solvent mixture THF-H_2O with 90% of THF: scale bar– 100 nm (left), scale bar – 50 nm (right).

Cryo-TEM analysis of PAA-*b*-PHS micelles in water is presented in Figure 16. The calculated micellar shape from shape factor was confirmed by cryo-TEM images. Small

number of spherical micelles was caused by the high aggregation number and low concentration of studied samples (< 1 mg/ml).

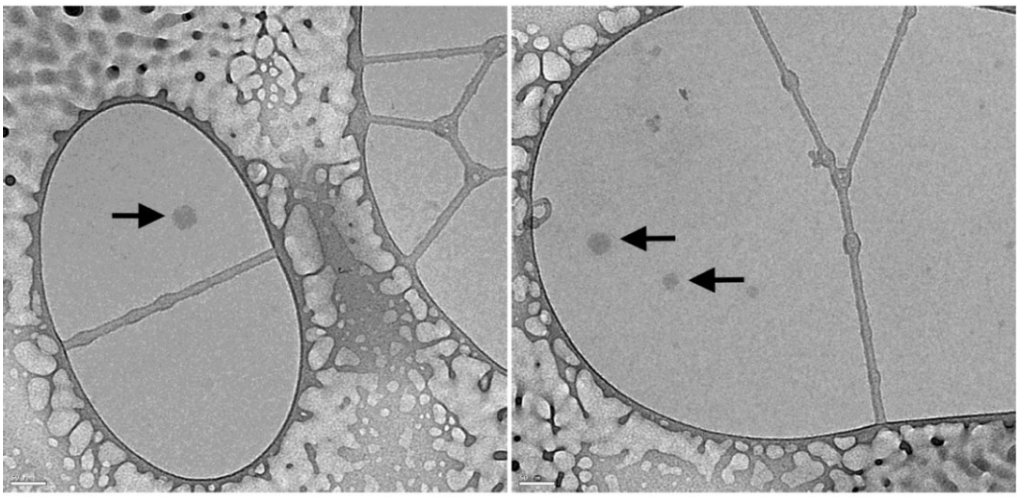

Figure 16 Cryo-TEM of spherical PAA-*b*-PHS micelles from initial solvent mixture THF-H_2O with 90% of THF: Scale bar – 50 nm.

The dissolution of PAA-*b*-PHS and PAA-*b*-PHS-*b*-PSC in same solvent mixture composition with 90% of THF content yielded two different morphologies: spherical micelles (diblock) and wormlike particles (triblock). The difference in architecture was due to the extra hydrophobic PSC block in PAA-*b*-PHS-*b*-PSC triblock terpolymer.

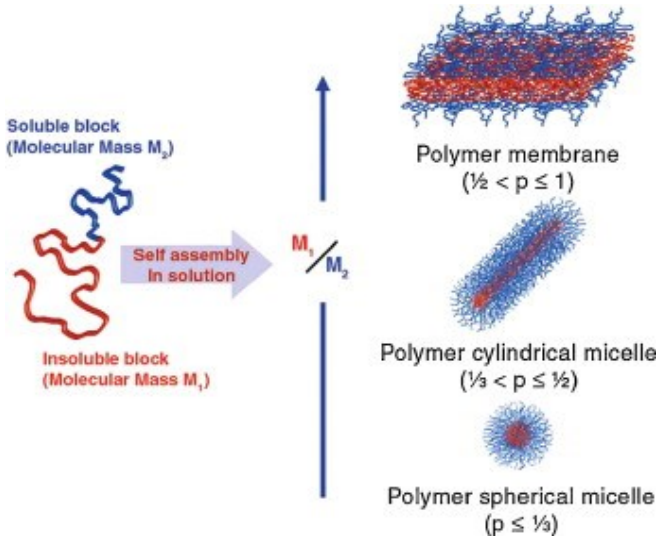

Figure 17 Influence of the volume ratio, approximated by the molecular weight ratio *P* of solvophobic and solvophilic blocks on obtained self-assembled morphology from block copolymers. [34]

The morphologies based on microphase separation of block copolymers both in bulk and in selective solvents have been described extensively by mean-field lattice theories such as Flory-Huggins theory. The predictions are based on taking into account the entropy term (related mostly to the conformation of macromolecular chains and their volume ratios) and the enthalpy term that is related to interaction of the segment pairs (segments of individual blocks and solvent). In the simple prediction describing the microphase separated system far beyond the strong segregation limit, the mutual segment-segment interaction is neglected and the morphology is given by the volume ratio of solvophobic and solvophilic blocks (Figure 17). The volume ratios are usually replaced by molar mass of the block. In our case the PAA_{85}-*b*-PHS_{17} diblock copolymer and PAA_{85}-*b*-PHS_{17}-*b*-PSC_5 triblock terpolymer compositions provide the following ratios of solvophobic vs. solvophobic + solvophilic blocks, *P*, where molecular weights of the block are as follows: PAA(6120)-*b*-PHS(2040)-*b*-PSC(1305) and PAA(6120)-*b*-PHS(2040). For diblock, *P* = PHS/(PAA+PHS) = 0.25; and for triblock in 10% THF-water mixtures, *P* = (PHS+PSC)/(PAA+PHS+PSC) = 0.35. Although the number of PSC segments is fairly low, due to the bulkiness of the carborane moieties the volume fraction of the PCS block is relatively significant. The estimated fractions are in line with the observed morphologies (spherical micelles for $P < 1/3$ in Figure 16; and cylindrical micelles for $1/3 < P < 1/2$ in Figures 11 and 15).[34] Because the value of *P* ratios depends on the weight of the solvophobic block, it depends also on the solvent mixture. These effects are evident for the micelles prepared in THF-water mixtures with relatively high content of THF. Because THF is better solvent for PHS than for PSC, it leads to the decrease of the ratio *P* leading to the spherical morphology of the micelles (Figures 13 and 15).

5.3. Studies on fluorophores solubilization in nanoparticles by fluorescence spectroscopy

The major difference between PAA-*b*-PHS-*b*-PSC and PAA-*b*-PHS micelles is the presence of two hydrophobic core domains with different inner environments achieved from triblock terpolymer self-assembly. Steady-state and time-resolved fluorescence with use of 2 hydrophobic fluorophores, 2-methyl naphthalene, (N) and carborane-methoxycoumarin conjugate fluorescence probe, (CBMC), were chosen as suitable

methods to distinguish multiple compartments of triblock terpolymer micelles. The emission spectra and fluorophore lifetime are highly sensitive to surrounding conditions and possible presence of another emitting species in near proximity of analyzed fluorophore. Also, an overlap between N emission spectra and CBMC excitation spectra showed promise in way to distinguish multiple micellar environments by fluorescence energy transfer. Fluorescence studies of prepared micellar solutions were based on hypothetical assumptions, among them: (i) the triblock terpolymer self-assembly should yield multicompartment nanoparticles; (ii) N and CBMC fluorescence probes in near proximity should undergo energy transfer upon excitation of N; (iii) the localization of individual probes in different micellar compartments of triblock terpolymer micelles should make the energy transfer between N and CBMC impossible; (iv) the energy transfer should occur in diblock copolymer micelles due to the co-localization of the probes in the same hydrophobic compartment.

Considering the hydrophobic properties of both fluorophores, the migration of N and CBMC from aqueous solution to the hydrophobic micellar core is expected. While the coexistence of N and CBMC in one common environment, such as hydrophobic core of diblock copolymer micelle, the fluorescence energy transfer between two fluorophores was predicted in manner that N acts as donor and CBMC as acceptor. The near proximity of donor and acceptor molecules, as a principal requirement of energy transfer would not be achievable in the case of fluorophores located in different hydrophobic compartments; hence the energy transfer should not occur if the probes are selectively located in different compartments.

Fluorescence studies of micelles characterization were performed in sequence of experiments as described in Figure 18, starting with *emission spectra measurement 1* of pure micellar solutions with an equal amount of energy transfer donor or acceptor. The exact number of individual fluorophores per micelle was determined from micellar concentration obtained by SLS measurements.

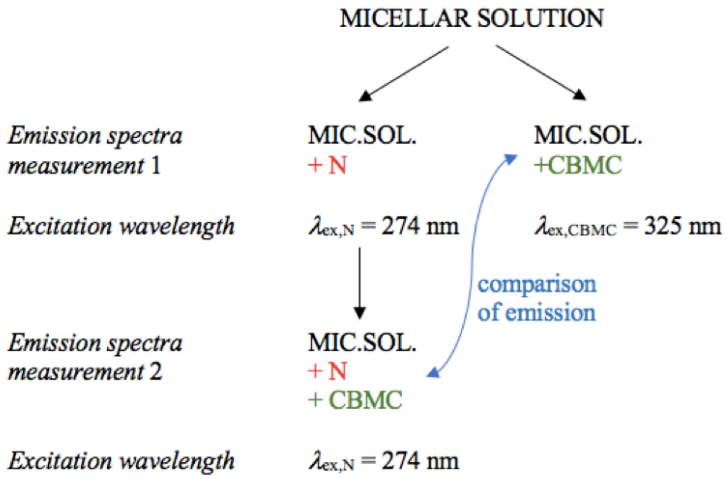

Figure 18 Emission spectra measurements divided into two experiments, showing the composition of measured solution mixtures, used fluorophores and excitation wavelength for individual measurements. The probe concentrations were: CBMC – 0.1 μM; N – 0.01 μM for all samples.

First (*emission spectra measurement 1*), the emission spectra of fluorophores were analyzed at their respective excitation maxima: 2-methyl naphthalene - $\lambda_{ex,N}$ = 274 nm and coumarin-carborane probe - $\lambda_{ex,CBMC}$ = 325 nm. Then (*emission spectra measurement 2*), donor and acceptor fluorophores were added into the micellar solution in a ratio of 20:40, (N:CBMC). Micelles were then excited at $\lambda_{ex,N}$ and the emission spectra was compared with emission spectra of micellar solution containing only donor.

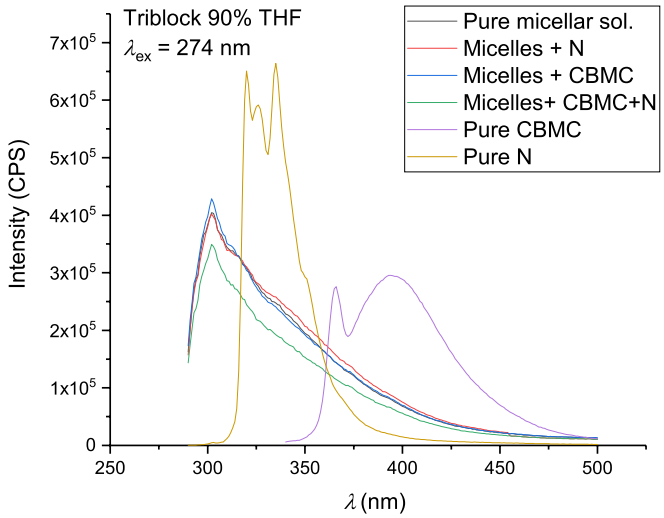

Figure 19 Emission spectra *of* PAA-*b*-PHS-*b*-PSC (triblock) from initial solvent mixture with 90% of THF*:* Individual emission spectra of micellar solutions containing fluorophores, compared with the emission of pure micelles (λ_{ex} = 274 nm). For comparison: N and CBMC emission spectra in water after excitation at 274 nm and 325 nm, respectively. The probe concentrations were: CBMC – 0.1 μM; N – 0.01 μM for all samples.

Emission spectra of pure fluorophores in water were compared with *emission spectra measurement 1* and *2*, see Figure 19. An unexpected intrinsic fluorescence of micelles complicated the analysis of emission spectra. Figure 19 shows identical emission of pure micellar solution and micellar solutions containing fluorophores (N, CBMC, and N + CBMC). The emission of pure N and CBMC solutions were included to the same graph for comparison. It is clear that N and CBMC emission is missing in the micellar solutions.

Time-resolved measurement of the N + CBMC probes in the micellar solution upon the excitation at λ_{ex} = 282 nm by the nanoLED source was compared with life-time of intrinsic emission of the pure micellar solution, see Figure 20. The identical fluorescence decays were obtained for both pure micellar solution and solution containing probes. Further, both decays almost overlap with the instrument response function (Prompt). The small maxima around 12 ns in Figure 20 are property of the laser diode source and cannot be removed. The lifetime of micelles and micelles containing both fluorophores was found identical, without any effect of used fluorophores. The lifetime of intrinsic micellar fluorescence was obtained from fitting by two-exponential function with the one component $\tau \approx 1$ ns, which can be assigned to intrinsic fluorescence of the micelles, and the second component that was unrealistically low and can be assigned to the scattering. The strong overlap of the fluorescence decays with the laser diode profile is caused by insufficient separation of the intensive scattering of the micelles and the weak fluorescence signal. Both experiments were repeated with doubled amount of fluorophore per micelle. No difference in emission or lifetime was observed.

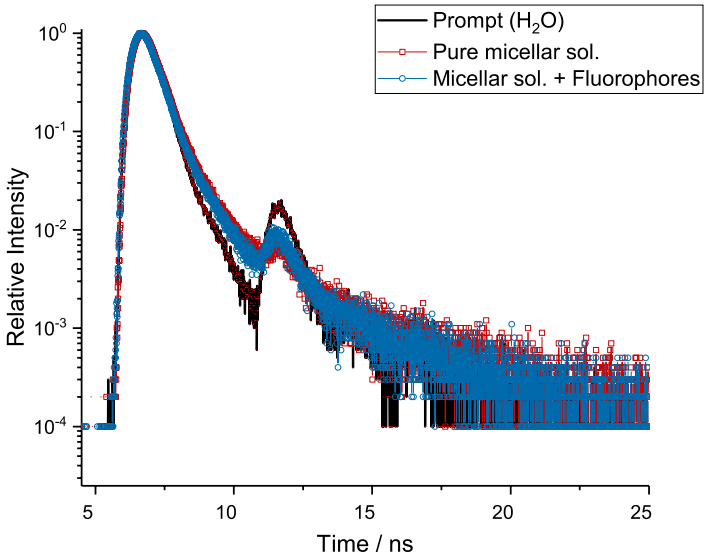

Figure 20 Time-resolved fluorescence decays, λ_{ex} = 282 nm, of (red points) pure PAA-*b*-PHS-*b*-PSC micelles (with initial THF-H_2O of 90% THF) and (blue points) PAA-*b*-PHS-*b*-PSC micelles mixture with N + CBMC; the instrument response function (Prompt) measured with pure water is included as black line – the second maximum observed around 12 ns is an inherent property of the pulse source that cannot be removed.

The absence of fluorophore emission was attributed to the polymer chain composition. The lack of fluorescence signal of N and CBMC fluorophores can be explained by the significant cut-off effect of pure micellar solutions. Micellar solutions absorb the excitation pulses around λ = 285 nm and λ = 325 nm. These are in the regions of N and CBMC excitation bands. Another explanation of the efficient quenching of the probe emission is the presence of free radicals within the PHS compartments as described below.

5.3.1. Crosslink of hydroxystyrene molecules

Unexpected detection of the intrinsic micellar fluorescence and yellowish color of the micellar solutions exposed to irradiation as well as disappearance of N and CBMC emission in the micellar systems led to further fluorescence studies. Analysis of the emission spectra after excitation at λ_{ex} = 274 nm shown two fluorescence bands, the first at λ_{em} = 302 nm and the second at λ_{em} = 365 nm for PAA-*b*-PHS-*b*-PSC micelles (triblock), and λ_{em} = 310 nm and λ_{em} = 365 nm for PAA-*b*-PHS micelles (diblock). The second band was observed also after the excitation of micellar solution at λ_{ex} = 325 nm.

Emission spectra of PAA-*b*-PHS-*b*-PSC and PAA-*b*-PHS micelles are presented in Figure 21 at various excitation wavelengths.

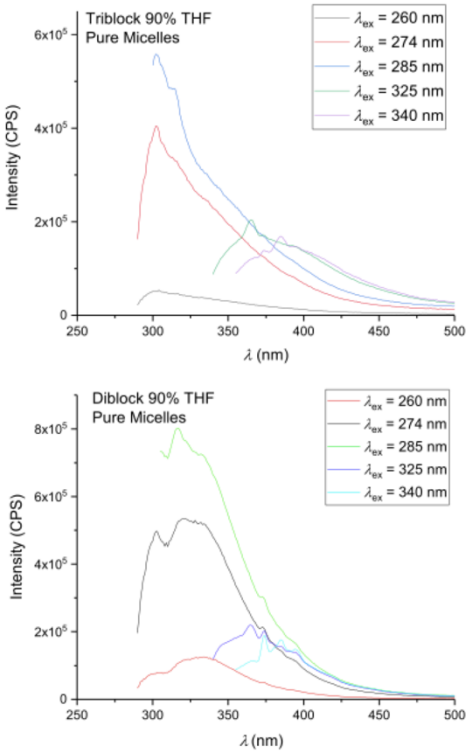

Figure 21 The superposition of emission spectra of PAA-*b*-PHS-*b*-PSC (triblock) and PAA-*b*-PHS (diblock), from the initial THF-H_2O mixture of 90% THF, at various excitation wavelengths as indicated in the graphs. Two main emission maxima were detected: 302 nm and 365 nm for triblock, and 310 nm and 365 nm for diblock.

Various studies of poly(hydroxystyrene) and polystyrene both in solution and in thin films show their intrinsic fluorescence as well as the possibility of the formation of colored quinoid structures upon photoexcitation leading to the PHS crosslinking.[35,36,37,38,39] The possible mechanisms of the crosslinking reaction are shown in Figure 22. These photo-initiated process can explain the yellowish color of the micellar solution.[36] The formation of free radical can also explain the quenching of the N and CBMC fluorescence.

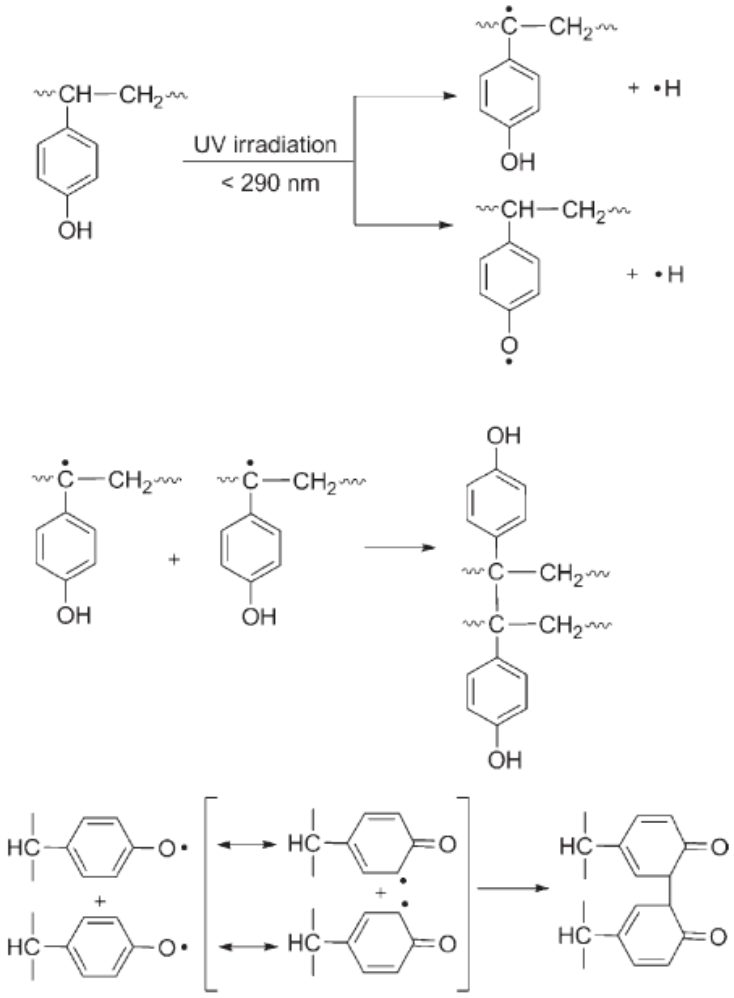

Figure 22 Proposed mechanism of crosslinking reactions of the PHS block upon the UV irradiation.[35]

Two fluorescence bands in emission spectra of PAA-*b*-PHS-*b*-PSC and PAA-*b*-PHS micelles can be caused by PHS block fluorescence. The emission spectra of PHS, Figure 23 (left, top), shows similar emission maxima at 310 nm and 360 nm[36] that were observed in PAA-*b*-PHS-*b*-PSC and PAA-*b*-PHS micellar solutions, Figure 23 (right). We assume no presence of the fluorescent impurity because of the reproducibility of the fluorescence spectra for several samples and relatively high fluorescence intensity.

The fluorescence band around 310 nm is usually attributed to luminescence of PHS monomer, while the second band around 350 nm can be assigned to formation of excimer or fluorescent dimer depending on the polymer regularity and tacticity.[36,37] The monomer-excimer emission ratio of PHS in methanol solutions depends also on the sample temperature, Figure 23 (left).

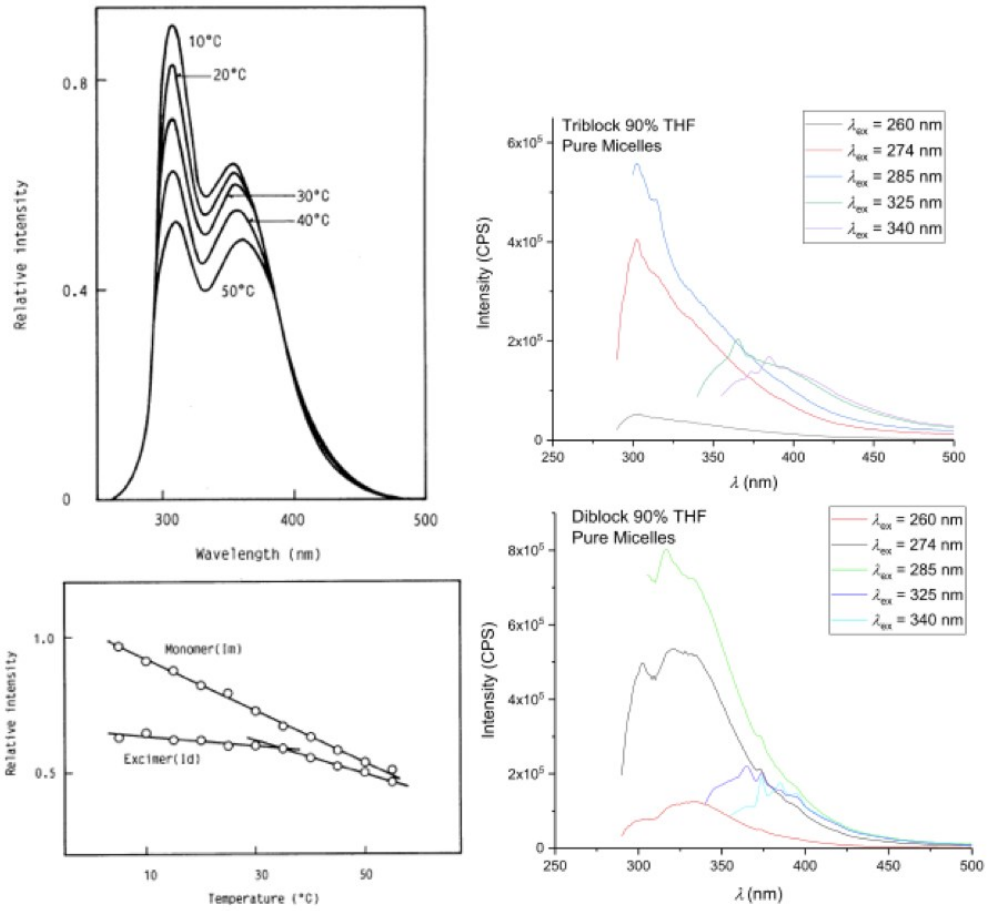

Figure 23 The comparison of PHS monomer and excimer emission: (left, top) Emission spectra of PHS in methanol at 25 °C, (left, bottom) Excimer-monomer ratio dependence on temperature,[37] with the luminescence of the studied micelles: (right, top) Emission spectra of pure micellar solution of PAA-*b*-PHS-*b*-PSC from initial solvent mixture with 90% of THF, (right, bottom) Emission spectra of pure micellar solution of sample PAA-*b*-PHS from initial solvent mixture with 90% of THF.

6. Conclusion

1. PAA-*b*-PHS-*b*-PSC triblock terpolymer micelles were prepared in tetrahydrofuran-water solution mixtures followed by the transfer to water and aqueous buffers, all in a controlled manner. The solubility of PAA-*b*-PHS-*b*-PSC markedly increases with increasing tetrahydrofuran portion in solvent mixture. For comparison, PAA-*b*-PHS diblock copolymer micelles were prepared under the same conditions.
2. By use of static and dynamic light scattering it has been proven that chosen micelle preparation process provides reproducible results concerning both micellar stability and hydrodynamic radii of the micelles. Increasing volume fraction of tetrahydrofuran in tetrahydrofuran-water solvent mixture influence micellar size in non-linear manner. The micellar shapes estimated according to $\frac{R_g}{R_H}$ and solvophobic-to-solvophilic block mass ratios were confirmed by cryo-TEM micrographs describing micelles with different shapes including: spherical micelles, oblate ellipsoids and wormlike micelles. Low contrast of individual micellar blocks and short core forming block did not allow to directly visualizing all three compartments of the triblock micelles by cryo-TEM: PAA shell was not visible due to the low contrast, and PHS and PSC compartments were indistinguishable. The segregation of PHS and PSC block was indirectly confirmed by different size and morphology of the triblock micelles prepared from different THF-water mixtures as THF acts as better solvent for PHS than for PSC.
3. Fluorescence studies (steady-state and time-resolved fluorescence) with 2-methylnaphthalene, N, and carborane-7-methoxycoumarin conjugate, CBMC, probes as fluorophores were carried out with PAA-*b*-PHS-*b*-PSC and PAA-*b*-PHS micelles. N and CBMC probes were assumed to solubilize within the PHS and PSC compartments with different partitioning. However, composition properties of polymer, among them the presence of PHS segments that are capable to absorb the excitation pulse and produce free radicals, deteriorated the detection of fluorescence emission from the probes. The fluorescence energy transfer between two fluorophores which was supposed to occur in core-corona PAA-*b*-PHS micelles did not appear. Thus, experimental verification of PAA-*b*-

PHS-*b*-PSC micellar compartments by fluorescence energy transfer could not be confirmed. Multiple fluorescence maxima and lifetime of analyzed micellar solutions were further studied in pure solutions without fluorophores content. The change in color has proven the presence of photochemically initiated crosslinking reaction between hydroxyl groups of PHS block in PAA-*b*-PHS-*b*-PSC and PAA-*b*-PHS micellar systems. The formation of radical might cause the quenching of the N and CBMC fluorescence. The steady-state and time-resolved study of PAA-*b*-PHS-*b*-PSC and PAA-*b*-PHS micelles revealed the intrinsic fluorescence of the micelles with fluorescence lifetime around 1 ns. Two bands at 302 nm and 365 nm can be assigned to fluorescence of PHS unimers and excimers, respectively, depending on the polymer conformation.

Because the compartments were not directly confirmed and fluorescence emission of N and CBMC probes were not detected in the studied micelles, we are planning further study on partitioning of small molecules in multicompartmentalized systems by fluorescent techniques and cryo-TEM visualization with intention of technical improvement towards the possible medical application in upcoming years.

Acknowledgment

This study is a part of a financially supported project by the Czech Science Foundation (GAČR), grant 17-00289Y.

7. References

1. Moughton, A. O.; Hillmyer, M. A.; Lodge, T. P. *Macromolecules* **2011**, *45* (1), 2-19.

2. Bates, C. M.; Bates, F. S. *Macromolecules* **2016**, *50* (1), 3-22.

3. Tritschler, U.; Pearce, S.; Gwyther, J.; Whittell, G. R.; Manners, I. *Macromolecules* **2017**, *50* (9), 3439-3463.

4. Nagarajan, R. *ACS Symposium Series Amphiphiles: Molecular Assembly and Applications* **2011,** 1-22.

5. Jones, M.-C.; Leroux, J.-C. *European Journal od Pharmacautics and Biopharmaceutics* **1999**, *48* (2), 101-111.

6. Deepak, V. D.; Sundararajan, P. R. *The Journal of Physical Chemistry B* **2011**, *115* (26), 8458-8464.

7. Marsat, J. -N,; Heydennreich, M.; Kleinpeter, E.; Berlepsch, H. V.; Böttcher, Ch.; Lachewsky, A. *Macromolecules* **2011**, *44* (7), 2092-2105.

8. Sun, G.; Cui, H.; Lin, L. Y.; Lee, N. S.; Yang, C.; Neumann, W. L.; Freskos, J. N.; Shieh, J. J.; Dorshow, R. B.; Wooley, K. L. *Journal of the American Chemical Society* **2011**, *133* (22), 8534-8543.

9. Holder, S. J.; Sommerdijk, N. A. J. M. *Polymer Chemistry* **2011**, *2* (5), 1018.

10. Uchman, M.; Štěpánek, M.; Procházka, K.; Mountrichas, G.; Pispas, S.; Voets, I. K.; Walther, A. *Macromolecules* **2009,** *42* (15), 5605-5613.

11. Wyman, I. W.; Liu, G. *Polymer* **2013**, *54* (8), 1950-1978.

12. Schärtl Wolfgang. *Light scattering from polymer solutions and nanoparticle dispersions;* Springer: Berlin, 2010.

13. Øgendal, L. H. *Light Scattering Demystified: Therory and Practice;* University of Copenhagen, 2017.

14. Gracia, C.; Gómez-Barreiro, S.; González-Pérez, A.; Nimo, J.; Rodríguez, J.r. *Journal od Colloid and Interface Science* **2004**, *274* (2), 408-413.

15. Brewer, A. K.; Striegel, A. M. *The Analyst* **2011**, *136* (3), 515-519.

16. Tande, B. M.; Wagner, N. J.; Mackay, M. E.; Hawker, C. J.; Jeong, M. *Macromolecules* **2001**, *34* (24), 8580-8585.

17. Lakowicz, J. R. *Principles of fluorescence spectroscopy*, 2nd ed.; Springer: New York, 2006.

18. Williams, A. T. R. *An Introduction to fluorescence spectroscopy;* Perkin-Elmer: Beaconsfied, 2000.

19. Albani, J. R. *Principles and applications of fluorescence spectroscopy*; Blackwell Science: Oxford, 2007.

20. Chasteen, G. T; Sam Houston State University, Huntsville, Texas.

21. Carroni, M.; Saibil, H. R. *Methods* **2016**, *95*, 78-85.

22. Milne, J. L. S.; Borgnia, M. J.; Bartesaghi, A.; Tran, E. E. H.; Earl, L. A.; Schauder, D. M.; Lengyel, J.; Pierson, J.; Patwardhan, A.; Subramaniam, S. *FEBS Journal* **2012**, *280* (1), 28-45.

23. Schacher, F.; Walther, A.; Müller, A. H. E. *Langmuir* **2009**, *25* (18), 10962-10969.

24. Tibbitt, M. W.; Dahlman, J. E.; Langer, R. *ChemInform* **2016**, *47* (19).

25. Sun, P.; Chen, D.; Deng, H.; Wang, N.; Huang, P.; Jin, X.; Zhu, X. *Bioconjugate Chemistry* **2017**, *28* (5), 1470-1480.

26. Torrice, M. *ACS Central Science* **2016**, *2* (7), 434-437

27. Nakamura, Y.; Mochida. A.; Choyke, P. L.; Kobayashi, H. *Bioconjugate Chemistry* **2016**, *27* (10), 2225-2238.

28. Haag, R.; Kratz, F. *Angewandte Chemie* **2016**, *45*, 1198-1215.

29. Zhenm Z.; Tang, W.; Chuang, Y.-J.; Todd, T.; Zhang, W.; Lin, X.; Niu, G.; Liu, G.; Wang, L.; Pan, Z.; Chen, X.; Xie, J. *ACS Nano* **2014**, *8* (6), 6004-6013.

30. Maeda, H. *Bioconjugate Chemistry* **2010**, *21* (5), 797-802.

31. Yura, Y.; Fujita, Y. *Oral Science International* **2013**, *10* (1), 9-14.

32. Barth, R. F.; Coderre, J. A.; Vicente, M. G. H.; Blue, T. E.; Miyatake, S.-I. *Current Clinical Oncology High-Grade Gliomas* 431-459.

33. Ferrer-Ugalde, A; Juárez-Pérez, E. J.; Teixidor, F.; Viñas, C.; Sillanpää, R.; Pérez-Inestrosa, E.; Núñez, R. *Chemistry – A Eropean Journal* **2011**, *18* (2), 544-553.

34. Kim, J. J.; Yang, S. Y.; Lee, Y.; Kim, Y. *Progress in Polymer Science* **2010**, *35* (11), 1325-1349.

35. Uppalapati, S.; Chada, S.; Engelhard, M. H.; Yan, M. *Macromolecular Chemistry and Physics* **2010**, *211* (4), 461-470.

36. Weir, N.; Arct, J.; Farahani, M. *Polymer Degradation and Stability* **1985**, *13* (4), 361-375.

37. Himuro, S. *Polymer Journal* **1993**, *25* (12), 1223-1228.

38. Sano, T.; Uchiyama, A.; Sago, T.; Itagaki, H. *European Polymer Journal* **2017**, *90*, 114-121.

39. López-Gejo, J.; Glieman, H.; Schimmel, T.; Braun, A. M. *Photochemistry and Photobiology* **2005**, *5*, 948-954.